Molecular Therapy
Original Article

Silencing mouse circular RNA *circSlc8a1* by circular antisense *cA-circSlc8a1* induces cardiac hepatopathy

Nan Wu,[1] Feiya Li,[1] Weining Yang,[1] William W. Du,[1] Faryal Mehwish Awan,[1,2] Chao Zhang,[1] Juanjuan Lyu,[1] Sema Misir,[1] Kaixuan Zeng,[1] Esra Eshaghi,[1] and Burton B. Yang[1,3]

[1]Sunnybrook Research Institute, Toronto, ON M4N3M5, Canada; [2]Department of Medical Lab Technology, the University of Haripur (UOH), Haripur, Pakistan; [3]Department of Laboratory Medicine and Pathobiology, University of Toronto, Toronto, ON, Canada

Circular RNAs (circRNAs) are a group of non-coding RNAs with a unique circular structure generated by back-splicing. It is acknowledged that circRNAs play critical roles in cardiovascular diseases. However, functional studies of circRNAs were impeded due to lack of effective *in vivo* silencing approaches. Since most circRNAs are produced by protein-coding transcripts, gene editing typically affects the coding activity of the parental genes. In this study, we developed a circular antisense RNA (*cA-circSlc8a1*) that could silence the highly expressed circRNA *circSlc8a1* in the mouse heart but not its parental *Slc8a1* linear mRNA. Transgenic *cA-circSlc8a1* mice developed congestive heart failure resulting in a significant increase in the body weight secondary to peripheral edema and congestive hepatopathy. To further test the role of *circSlc8a1*, we generated transgenic mice overexpressing *circSlc8a1* and observed a protective effect of *circSlc8a1* in a pressure overload model. Mechanistically, we found that *circSlc8a1* translocated into mitochondria to drive ATP synthesis. While establishing a transgenic murine model for antisense-mediated circRNA silencing without interfering with the parental linear RNA, our finding revealed the essential role of *circSlc8a1* in maintaining heart function and may lay the groundwork of using the circular antisense RNA as a potential gene therapy approach for cardiovascular diseases.

INTRODUCTION

Circular RNAs (circRNAs) are a large class of covalently linked single-stranded RNAs. Abnormal elevation of circRNA levels is associated with the onset or progression of cardiovascular diseases.[1–3] A variety of circRNAs have been demonstrated to play critical roles in cardiovascular diseases, including cardiomyopathy, myocardial infarction, and artery diseases.[4–6] The circRNAs have been recognized as potential therapeutic targets and biomarkers in cardiovascular diseases.[7–9] Therefore, it is of great importance to investigate the roles of circRNAs in the development of cardiovascular diseases. Recently, some other non-coding RNAs, such as miRNAs and lncRNAs, have been successfully applied in RNA therapy in cardiovascular diseases.[10,11] However, RNA therapy targeting circRNAs in cardiovascular diseases is still in the early stages of investigation.[12]

The circRNAs are produced by linking a 5′ splice donor with an upstream 3′ splice acceptor by back-splicing of the linear transcripts. The circRNAs are thus resistant to exonuclease treatment and more stable than the linear RNAs. The circRNAs have been identified across the genome and most of them are derived from protein-coding genes.[13] Since circRNAs share a part of the exon sequences with the parental coding genes, the traditional methods for generating gene knockout mice are hardly applied to establish circRNA knockout models. The widespread use of genetic methods becomes limited in circRNA functional studies due to lack of effective tools for knocking out/down endogenous circRNAs *in vivo* without affecting the parental mRNAs. In the past several years, some important breakthrough progresses have been made on *in vivo* model studies in certain exceptional scenarios. A circRNA, Cdr1as, without detectable linear cognate mRNA was identified and the Cdr1as locus was successfully knocked out by using CRISPR-Cas9.[14] A circRNA, circNfix, whose expression depends on a super-enhancer, was knocked down by mutation of its transcription factor, Meis1.[5] Another study reported the knockdown of circRNAs using CRISPR-Cas13 by directly targeting the back-splicing junction (BSJ) region of the circRNA during mouse embryo preimplantation development.[15] Recently, removal of intronic cassettes was also reported to knockout the expression of *circZfp292* and consequently altered the endothelial flow response.[16] The more popular methods used to silence a circRNA are the short hairpin RNAs and small interfering RNAs that are complementary to the BSJ of the circRNA.[17,18]

Here, we developed a strategy to generate a circularized antisense RNA that is complementary to the complete sequence of a circRNA. We expected that this antisense RNA was able to form a stable

Received 19 July 2022; accepted 14 October 2022;
https://doi.org/10.1016/j.ymthe.2022.10.005.

Correspondence: Burton B. Yang, Sunnybrook Research Institute, 2075 Bayview Ave, Toronto, ON M4N 3M5, Canada
E-mail: byang@sri.utoronto.ca

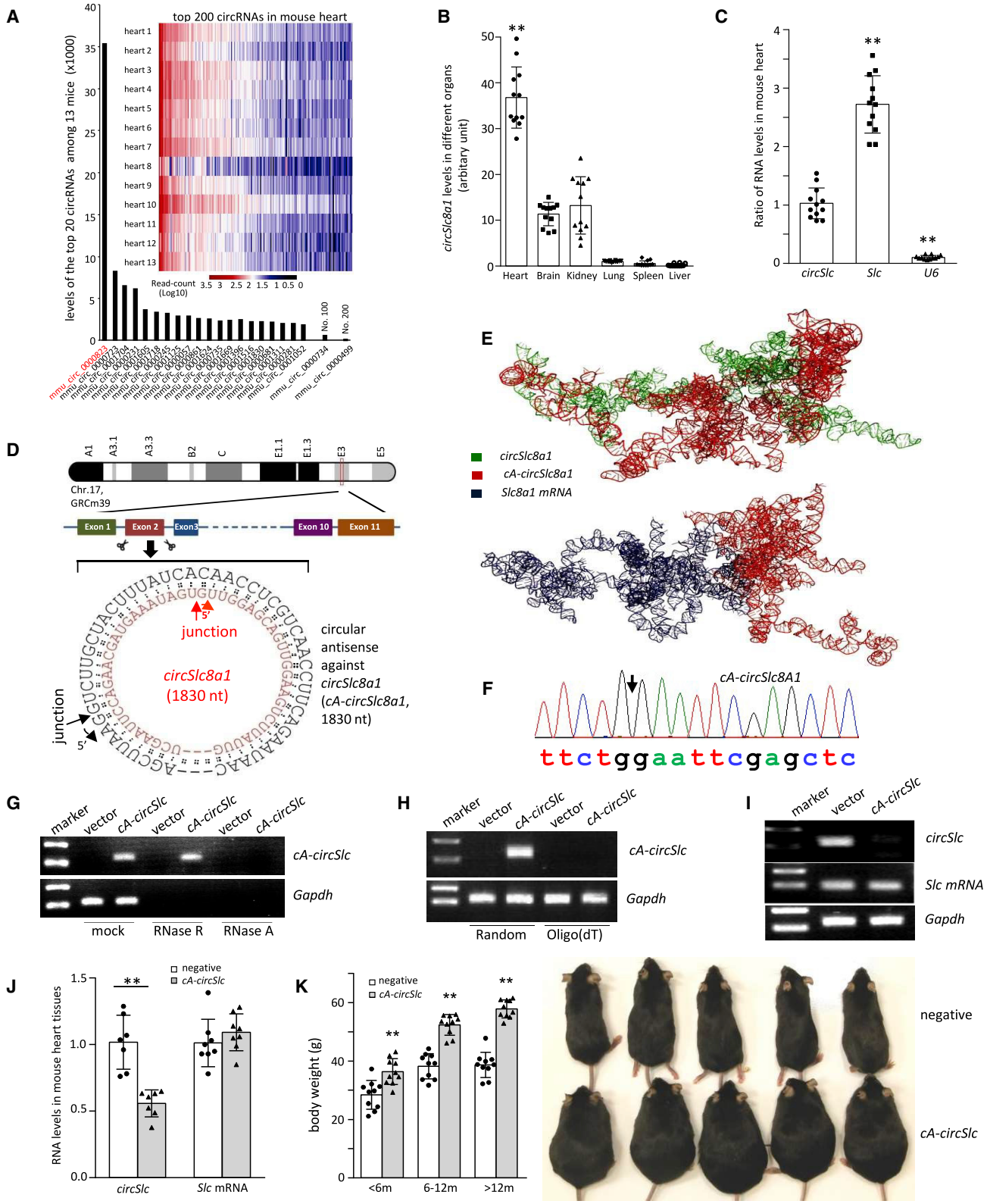

(legend on next page)

double-stranded RNA circle with its sense counterpart, resulting in the loss of the normal structure and functions of the sense circRNA. We first screened the circRNAs expressed in the mouse heart by RNA sequencing and selected the highest expressed circRNA, *circSlc8a1*, as our target. We then established a transgenic mouse model, in which the expression of *circSlc8a1*, but not the full-length *Slc8a1* mRNA and protein, was successfully sequestered by the circular antisense against *circSlc8a1* (*cA-circSlc8a1*) driven by a heart-specific promoter. We found that cardiac function in *cA-circSlc8a1*-transgenic mice was compromised, resulting in a significant increase in the body weight secondary to peripheral edema and the histological changes in the liver, including hepatic steatosis and cirrhosis. Importantly, our study demonstrates specific silencing of circRNA function. This proof-of-concept study may lay the foundation for potential clinical applications in circRNA therapy.

RESULTS

Blocking *circSlc8a1* expression by circular antisense RNA induces phenotypic changes

In this study, we perform high-throughput circRNA deep sequencing in myocardial tissue samples of 13 mice to search for the highest expressed circRNA in the hearts that may possess essential physiological functions. This allows us to develop an approach to silence the circRNA leading to a potent phenotype. We found that *circSlc8a1* (mmu_circ_0000823) was the topmost circRNA among 27,960 circRNAs detected in the hearts. Its expression levels (sequencing readcounts) were 4.2-fold of the second highest circRNA and even more than the sum by adding the readcounts of the top 2–8 circRNAs (Figure 1A). We examined the levels of *circSlc8a1* and linear *Slc8a1* mRNA in six main organs and found that both *circSlc8a1* and *Slc8a1* were expressed the highest in the heart compared with the other organs (Figures 1B and S1A). Furthermore, we compared the levels of *circSlc8a1* with *Slc8a1* mRNA and the housekeeping gene U6 in the mouse heart tissues and found that the expression levels of *circSlc8a1* in the heart were slightly lower than *Slc8a1* mRNA but higher than the housekeeping gene U6 (Figure 1C). In addition, 2,174 ± 313.82 copies of *circSlc8a1* per ng total RNA were determined in the mouse heart tissues by using droplet digital PCR. The high abundance of *circSlc8a1* implied its essential physiological role in the heart. Therefore, we designed a construct to express a circular antisense RNA (*cA-RNA*) perfectly complementary with *circSlc8a1*, named *cA-circSlc8a1*, which had the potential to sequester *circSlc8a1* by forming a sense-antisense double-stranded RNA circle (Figure 1D). The circular antisense was obtained by inserting the donor and acceptor sequences of the introns, respectively, into the antisense sequence of *circSlc8a1*, allowing back-splicing to form a circle. To validate whether *cA-circSlc8a1* has higher affinity to the *circSlc8a1* than to the linear *Slc8a1* mRNA, we used the computational docking methods to predict the potential blocking ability (Figure 1E). The docking score of *cA-circSlc8a1* complexed with *circ-Slc8a1* was found to be −7,621.32 kCal/mole, whereas the score was −1,699.97 kCal/mole for docking *cA-circSlc8a1* with the linear *Slc8a1* mRNA. Our results speculated that *cA-circSlc8a1* has much higher binding affinity with *circSlc8a1* compared with the linear *Slc8a1* mRNA.

Before further studying the function of *cA-circSlc8a1*, we first validated the successful circularization of *cA-circSlc8a1* plasmids in the cells. We transfected human HEK293 cells with the mouse *cA-circSlc8a1* plasmids and measured the expression of *cA-circSlc8a1* with mouse-specific divergent primers spanning the back-splice junction. The correct junction sequence that ectopically expressed in HEK293 cells was validated by Sanger sequencing as shown in Figure 1F. By pre-treatment prior to reverse transcription (RT) with RNase R (the enzyme that degrades linear RNAs but not circRNAs) and RNase A (the enzyme that degrades all RNAs), our results verified that *cA-circSlc8a1* was resistant to RNase R (Figures 1G and S1B). In addition, due to lack of open ends, the circRNAs cannot be reverse transcribed with oligo(dT) primers but only with random primers. Our PCR results showed that the *cA-circSlc8a1* plasmids formed circularized RNA, which could not be reverse transcribed with oligo(dT) primers (Figures 1H and S1C).

Figure 1. Generation of transgenic mice expressing circular antisense against *circSlc8a1* (*cA-circSlc8a1*) knocked down cardiac *circSlc8a1* and developed phenotypic changes

(A) RNA sequencing heatmap of differentially expressed circular RNA profiles in the heart of 13 mice. The highest readcount was *circSlc8a1* (mmu_circ_0000823), which was more than the sum obtained by adding the readcounts of the top 2–8 circRNAs. (B) Compared with the other organs analyzed, the heart expressed the highest level of *circSlc8a1*. n = 12; **p < 0.01 versus other organs. (C) The ratio of *circSlc8a1* (*circSlc*) in the mouse heart compared with *Slc8a1* (*Slc*) mRNA and ubiquitously expressed U6. n = 12; **p < 0.01 versus *circSlc*. (D) A diagram showing the sequence of the circular antisense against *circSlc8a1* (*cA-circSlc8a1*) that was perfectly complementary to *circSlc8a1*. (E) Graphical representation of the three-dimensional structure of *cA-circSlc8a1* and *circSlc8a1*, or *cA-circSlc8a1* and *Slc8a1* mRNA docked model visualized using PyMOL. (F) The back-splice junction of the ectopic mouse *cA-circSlc8a1* was validated by Sanger sequencing. (G) Representative images of *cA-circSlc8a1* expression with RNase R and RNase A treatment. A *cA-circSlc8a1* construct targeting mouse *circSlc8a1* was transfected into human HEK293T cells. The RNAs from vector or *cA-circSlc8a1*-transfected cells were treated with RNase R or RNase A followed by reverse transcription. The expression of *cA-circSlc8a1* was validated by mouse-specific primers against *cA-circSlc8a1*. n = 6. (H) Representative images of *cA-circSlc8a1* expression by using random or oligo(dT) primers for reverse transcription. A *cA-circSlc8a1* construct targeting mouse *circSlc8a1* was transfected into human HEK293T cells. The RNAs from vector or *cA-circSlc8a1*-transfected cells were reverse transcribed using random or oligo(dT) primers. The expression of *cA-circSlc8a1* was validated by mouse-specific primers against *cA-circSlc8a1*. n = 6. (I) Representative images of unbound *circSlc8a1* levels after transfection of *cA-circSlc8a1* in HL-1 cells. The RNAs from vector or *cA-circSlc8a1*-transfected cells were reverse transcribed using specific reverse primers for *circSlc8a1* followed by qPCR. n = 6. (J) The levels of *circSlc8a1* and *Slc8a1* mRNA in the heart of *cA-circSlc8a1*-transgenic mice. n = 8; **p < 0.01 versus negative. (K) Left, the body weight of *cA-circSlc8a1*(+) mice (*cA-circSlc*) was measured at different time points and compared with the age-matched *cA-circSlc8a1*(−) counterparts (negative) litters. **p < 0.01, n = 10. Right, a photo of *cA-circSlc8a1*(+) mice and their age-matched negative counterparts taken at the age of 10 months, showing an increase in the body weight in *cA-circSlc8a1*(+) mice.

To confirm that *cA-circSlc8a1* could block *circSlc8a1* without affecting *Slc8a1* mRNA *in vitro* before generating the transgenic mice, we transfected the *cA-circSlc8a1* plasmids in HL-1 cells, an immortalized mouse cardiomyocytes cell line. RT using random primers for both *circSlc8a1* and *cA-circSlc8a1* in transfected HL-1 cells may lead to misamplification of *cA-circSlc8a1* in the following qPCR analysis. To avoid this, we conducted gene-specific RT by using the reverse primer that was specifically complementary to *circSlc8a1*, and could not reverse transcribe *cA-circSlc8a1*. In addition, the reverse primer specific for *circSlc8a1* could not bind to those *circSlc8a1* that had already formed double-stranded RNA circle with *cA-circSlc8a1* for RT. Therefore, only the free unbound *circSlc8a1* could be detected by using the circRNA-specific RT with specific reverse primer followed by qPCR. Our results revealed that *circSlc8a1* was blocked by *cA-circSlc8a1* while the levels of *Slc8a1* mRNA were not affected (Figures 1I and S1D). Taken together, these results validated that *cA-circSlc8a1* plasmids successfully produced a circularized antisense RNA that blocked *circSlc8a1* without affecting *Slc8a1* mRNA in the cells.

To further validate the function of *cA-circSlc8a1 in vivo*, we established a transgenic mouse model expressing *cA-circSlc8a1* driven by a heart promoter to specifically silence *circSlc8a1* in the mouse heart (Figures S1E and S1F). We confirmed that the amount of free unbound *circSlc8a1* was significantly decreased in the heart of *cA-circSlc8a1*-transgenic mice (Figure 1J). Nevertheless, the *Slc8a1* mRNA and SLC8A1 protein expression in the heart of *cA-circSlc8a1*-transgenic mice were at the similar levels compared with the negative mice, which excluded the possibility that *cA-circSlc8a1* affected the parental *Slc8a1* expression (Figures 1J and S1G). Notable phenotypic changes were observed in these *cA-circSlc8a1*-transgenic mice compared with the litter-matched negative counterparts (Figures 1K and S1H). The body weights and the heart/tibia length ratio of *cA-circSlc8a1*-transgenic mice were significantly higher than those of the negative mice (Figures 1K and S2A).

Development of hepatic steatosis as a consequence of impaired heart function

Since the transgenic *cA-circSlc8a1* expression was cardiac specific, we examined whether the phenotypic changes were caused by the *cA-circSlc8a1* due to depleting endogenous *circSlc8a1* function in the heart. To test this, we evaluated the heart function of the *cA-circSlc8a1*-transgenic mice and their negative counterparts at different ages. Using the Vevo 2000 imaging system, we detected a significant malfunction in the *cA-circSlc8a1*-transgenic mice. Typical M-mode echocardiograms showed increased left ventricular chamber sizes and decreased ventricular contractile ability in the *cA-circSlc8a1*-transgenic mice compared with the litter-matched negative mice (Figure 2A). At the age of 6 months and above, *cA-circSlc8a1*-transgenic mice showed a significant decrease in the left ventricular ejection fraction (LVEF), left ventricular fractional shortening (LVFS), and left ventricular pressure (dp/dt) compared with the litter-matched negative mice (Figures 2B–2D). These transgenic mice showed increase in left ventricular end diastolic diameter (LVEDD) and left ventricular end systolic diameter (LVESD), leading to a decrease in LVEDD-LVESD (Figures S2B–S2D).

To corroborate the effect of *cA-circSlc8a1* on decreasing heart function, we further examined the morphological changes of the cardiac tissue in the transgenic mice. Hematoxylin and eosin (H&E) staining of the heart sections showed cardiac hypertrophy in the *cA-circSlc8a1*-transgenic mice at all time points (Figure 2E), consistent with the impaired heart functions, suggesting remodeling of the cardiac tissues. In support of this, we analyzed cardiac fibrosis by staining the heart sections with Masson's trichrome and Sirius red to visualize the collagen deposition and detected increased fibrotic staining in the *cA-circSlc8a1*-transgenic mouse heart (Figures 2E and S2E). Moreover, to examine cardiac hypertrophy, we stained cardiomyocytes with Alexa Fluor 555-conjugated wheat germ agglutinin (WGA) in the cross-section of the *cA-circSlc8a1*-transgenic and the litter-matched negative mouse hearts and detected enlargement of cardiomyocytes sizes in the *cA-circSlc8a1*-transgenic mice, reaching significant levels at all time points, far before cardiac fibrosis was observed (Figures 2E and S2F). We also confirmed cardiac hypertrophy in the *cA-circSlc8a1*-transgenic mice by measuring the expression of ANP and BNP, the markers of myocardial hypertrophy (Figure S2G).

In the *cA-circSlc8a1*-transgenic mice, we noticed that hepatic steatosis was developed as early as 3 months old. The lipid droplets were extensively accumulated in the liver of *cA-circSlc8a1*-transgenic mice before the age of 6 months, visualized by both H&E and Oil Red O (ORO) staining (Figure 3A). The lipid droplets were also quantified by ImageJ scanning (Figure S3A). Moreover, 2 out of 14 *cA-circSlc8a1*-transgenic mice at the age of 12 months showed significant liver cirrhosis while none of the negative mice did (Figure S3B). To validate whether such hepatic steatosis was caused by the ectopic cardiac-specific expression of *cA-circSlc8a1*, we examined the levels of *cA-circSlc8a1* precursor in different organs, including both heart and liver and detected a dramatic increase in *cA-circSlc8a1* precursor levels in the heart but not in the liver of the *cA-circSlc8a1*-transgenic mice (Figures 3B and S3C). In addition, we also used a probe specifically targeting *circSlc8a1* to pull down *circSlc8a1* in the heart and liver of *cA-circSlc8a1* transgenic and the litter-matched negative mice. Due to the formation of double-stranded RNA circle with *cA-circSlc8a1*, *circSlc8a1* could not bind to its specific probe that was complementary to its BSJ region in the presence of *cA-circSlc8a1* (Figure 3C). In the heart of *cA-circSlc8a1*-transgenic mice, significantly less *circSlc8a1* was pulled down by the *circSlc8a1* probe since *cA-circSlc8a1* blocked the binding of the *circSlc8a1* probe with the double-stranded circRNA (Figure 3D, left). However, such effects could not be observed in the liver of the *cA-circSlc8a1*-transgenic mice (Figure 3D, right). These findings confirmed that hepatic steatosis in the *cA-circSlc8a1*-transgenic mice originated from the heart dysfunction. In addition, to test the effect of the dsRNA-induced immune response, we examined the levels of multiple immune potentiated cytokines in the heart of *cA-circSlc8a1*-transgenic mice. Our results showed that, except for a slight increase in IL-6 expression, the expression of other cytokines

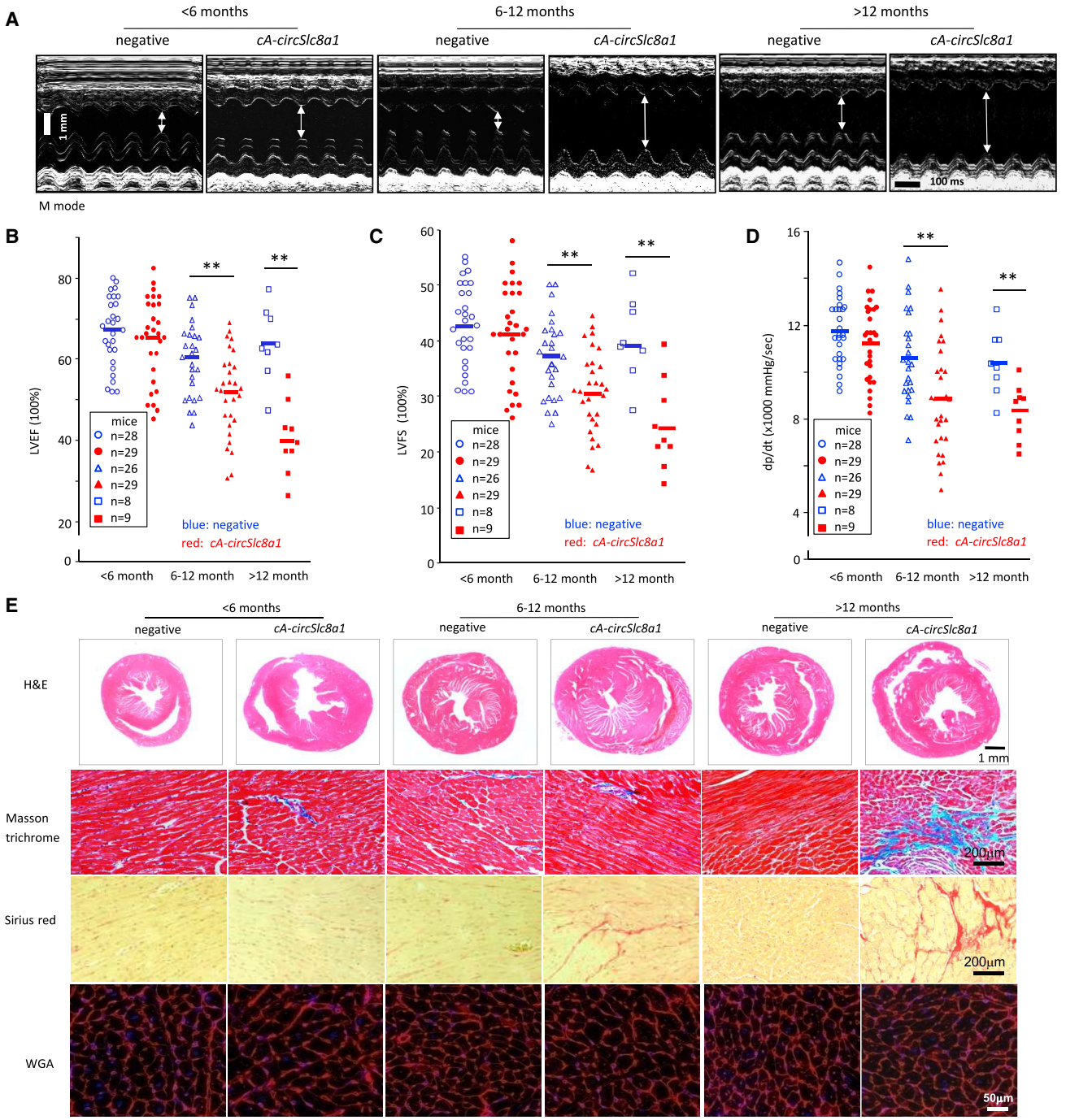

Figure 2. Heart function and cardiac histological changes of *cA-circSlc8a1*-transgenic mice evaluated by echocardiography and staining

(A) The representative echocardiography of *cA-circSlc8a1*-transgenic mice at different ages. (B) Echocardiography of *cA-circSlc8a1*(+) mice showed reduced left ventricular ejection fraction (LVEF) compared with the litter-matched negative mice. **p < 0.01 versus negative. (C) Echocardiography of *cA-circSlc8a1*(+) mice showed reduced left ventricular fractional shortening (LVFS) compared with the litter-matched negative mice. **p < 0.01 versus negative. (D) Echocardiography of *cA-circSlc8a1*(+) mice showed reduced left ventricular pressure (dp/dt) compared with the litter-matched negative mice. **p < 0.01 versus negative. (E) Representative photographs of Masson trichrome staining and Sirius red staining showing significant development of cardiac fibrosis in *cA-circSlc8a1*(+) mice after age 12 months. H&E staining and WGA staining showed development of cardiac hypertrophy in *cA-circSlc8a1*(+) mice as early as under age 6 months.

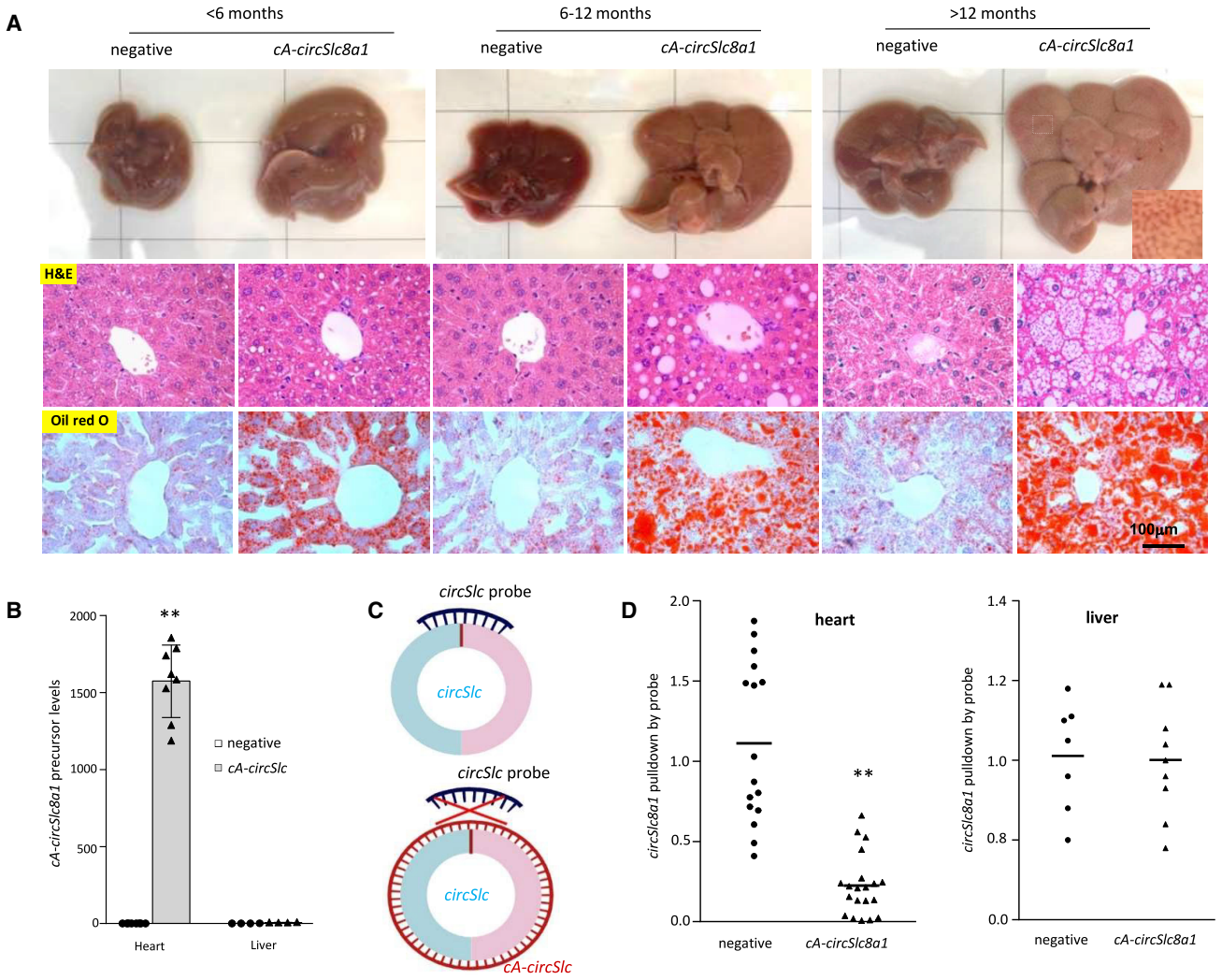

Figure 3. The *cA-circSlc8a1*-transgenic mice developed cardiogenic hepatic steatosis

(A) Representative photographs of gross appearance, H&E staining and Oil Red O staining of livers from *cA-circSlc8a1* mice at different ages, detecting hepatic steatosis in *cA-circSlc8a1*(+) mice. (B) The expression levels of *cA-circSlc8a1* precursor in the heart and liver of *cA-circSlc8a1*-transgenic mice, confirming specificity of the heart promoter. n = 8; **p < 0.01 versus negative heart. (C) A schematic illustration of the interaction of *circSlc8a1* probes to *circSlc8a1* with or without the presence of *cA-circSlc8a1*. (D) *circSlc8a1* was pulled down significantly less by the *circSlc8a1* probe in the heart (left) of *cA-circSlc8a1*(+) mice (**p < 0.01 versus negative), whereas no difference was observed in the liver (right) of *cA-circSlc8a1*(+) mice compared with the litter-matched negative mice. n = 16–20.

in *cA-circSlc8a1*-transgenic mice was at similar levels to those in negative mice (Figure S3D), excluding the effect of immune response on the observed phenotype. Thus, sequestering endogenous *circSlc8a1* by *cA-circSlc8a1* appeared to have instigated cardiac hypertrophy and malfunction, which consequently led to hepatic steatosis and eventually cirrhosis.

Transgenic expression of *circSlc8a1* prevents pressure overload-induced heart injury

Our results from *cA-circSlc8a1*-transgenic mice implied that *circSlc8a1* might play an essential role in maintaining the physiological function of the heart. Therefore, we constructed a *circSlc8a1* plasmid for performing further functional studies on *circSlc8a1*. We found that *circSlc8a1* could only be detected in cDNA but not in gDNA with divergent primers, while the linear form of *Slc8a1* could be detected in both cDNA and gDNA with convergent primers in HL-1 cells (Figure 4A). Our results also showed that the overexpressed *circSlc8a1* was resistant to RNase R treatment (Figures 4B and S4A) and could not be reverse transcribed with oligo(dT) primers (Figures 4C and S4B). In addition, the BSJ sequences of *circSlc8a1* were verified in the PCR products from *circSlc8a1* overexpressed HEK293 cells by Sanger sequencing (Figure 4D). All of these results validated the successful circularization of *circSlc8a1* plasmid that we constructed.

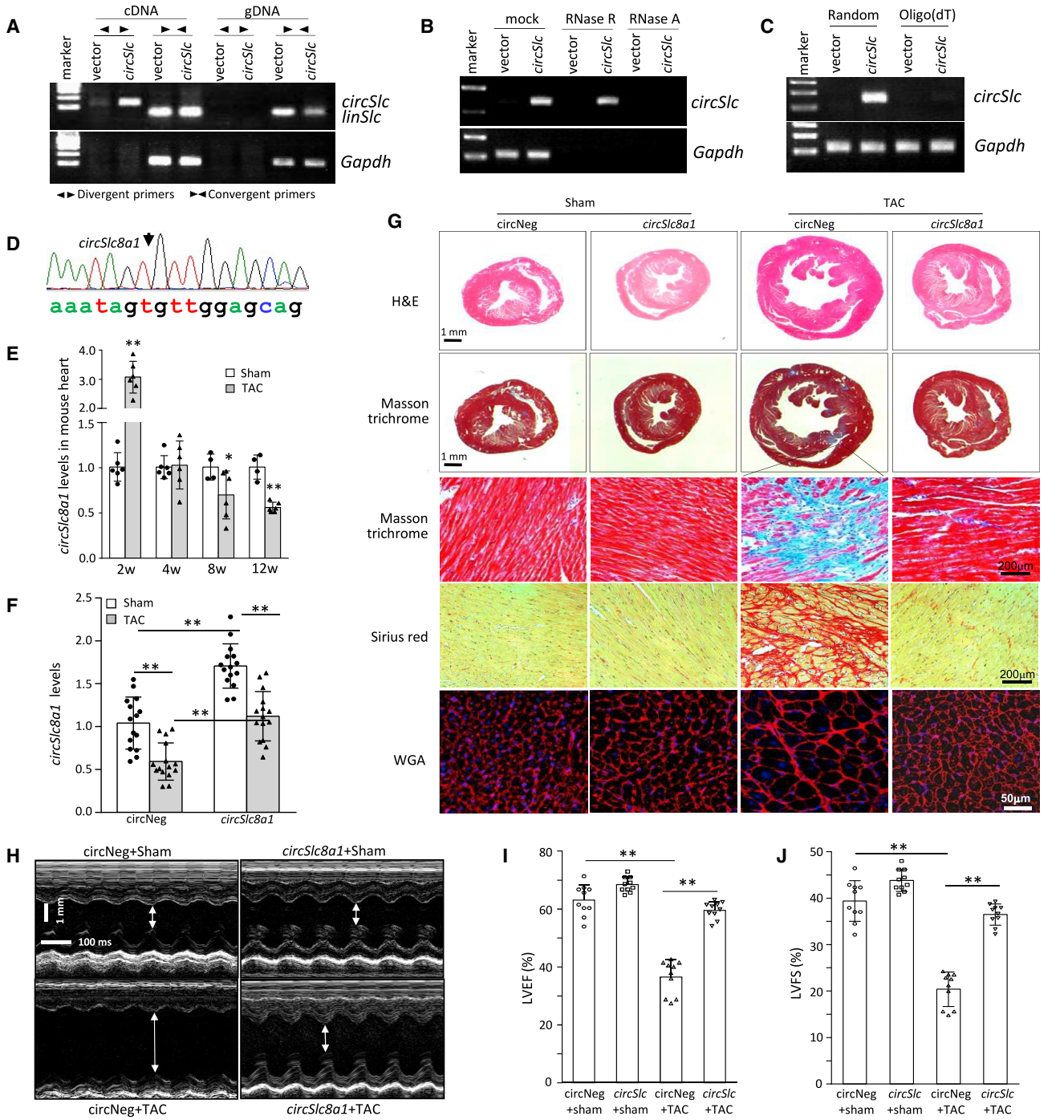

Figure 4. Transgenic expression of *circSlc8a1* improved heart function against transverse aortic constriction-induced pressure overload

(A) The *circSlc8a1* plasmids were transfected into HL-1 cells followed by RT-qPCR. *circSlc8a1* was amplified by divergent and convergent primers in cDNA, and by convergent primers only in gDNA. (B) The *circSlc8a1* plasmids were transfected into human HEK293T cells. The RNAs from vector or *circSlc8a1*-transfected cells were treated with RNase R or RNase A followed by reverse transcription. The expression of *circSlc8a1* was validated by using mouse-specific primers against *circSlc8a1*. n = 4. (C) Representative images of *circSlc8a1* expression by using random or oligo(dT) primers for reverse transcription. The *circSlc8a1* plasmids were transfected into human HEK293T cells. The RNAs from vector or *circSlc8a1*-transfected cells were reverse transcribed using random or oligo(dT) primers. The expression of *circSlc8a1* was validated by using mouse-specific primers against *circSlc8a1*. n = 6. (D) The back-splice junction of the ectopic mouse *circSlc8a1* construct was confirmed by Sanger sequencing. The *circSlc8a1* expression construct was used to generate transgenic mice. (E) The levels of *circSlc8a1* were significantly decreased in the mouse heart tissues at 8–12 weeks

(legend continued on next page)

We then conducted transverse aortic constriction (TAC) surgery in the mice to induce pressure overload (PO) and the subsequent cardiac hypertrophy and heart failure. The expression of *circSlc8a1* in the wild-type mice was increased at 2 weeks post-TAC surgery while it decreased significantly 8–12 weeks after TAC surgery in the heart of TAC mice compared with the sham mice (Figure 4E), which suggested that loss of *circSlc8a1* could be associated with PO-induced heart failure. Based on these results, we established a *circSlc8a1*-transgenic mouse line (Figure S4C). The *circSlc8a1*-transgenic mice and their negative counterparts were then subjected to TAC surgery to confirm the roles of *circSlc8a1 in vivo*. While TAC surgery significantly decreased *circSlc8a1* levels in the heart, transgenic expression of *circSlc8a1* was able to maintain *circSlc8a1* levels as high as those similar to negative sham mice (Figure 4F). Upon 12 weeks PO induced by TAC, the *circSlc8a1*-transgenic mice showed significantly less cardiac hypertrophy and fibrosis along with higher levels of *circSlc8a1* in the heart compared with the litter-matched negative controls (Figures 4G, S4D, and S4E). In addition, the levels of hypertrophy markers (ANP and BNP) and fibrosis markers (collagen-I and collagen-III) were significantly lower in the hearts of the *circSlc8a1*-transgenic mice compared with the negative controls upon PO (Figures S5A and S5B).

Echocardiography analysis showed that TAC surgery remarkably increased the left ventricular chamber size that was prevented by transgenic expression of *circSlc8a1* (Figure 4H). In cardiac functional measurements, TAC surgery significantly impaired the heart function of the negative mice, while the heart function of the *circSlc8a1*-transgenic mice was maintained at similar levels to the negative mice in the sham group (Figures 4I, J, and S5C–S5F). These results demonstrated the protective effects of *circSlc8a1* during heart injury and indicated the importance of *circSlc8a1* in maintaining physiological heart function.

The cA-circSlc8a1 induces cardiac hypertrophy and hepatic steatosis via sequestering cardiac *circSlc8a1*

To further validate that the phenotypic changes in *cA-circSlc8a1*-transgenic mice were through its specific effects on sequestering *circSlc8a1*, we generated a double transgenic mouse line by ectopically expressing both *circSlc8a1* and *cA-circSlc8a1* (Figures S6A–S6C). In the heart of double transgenic mice, the levels of *circSlc8a1* were maintained at similar levels to the negative mice, which were verified by both gene-specific RT-qPCR and RNA pull-down assay (Figures 5A and 5B), while the *Slc8a1* mRNA was not affected in these mice (Figure S6D). Regarding the phenotypes, we found that the body weight increase in the *cA-circSlc8a1*-transgenic mice was effectively reversed by re-introducing *circSlc8a1* into the mice to generate double transgenic mice (Figure 5C). In addition, cardiac hypertrophy in the *cA-circSlc8a1*-transgenic mice was not observed in the hearts of double transgenic mice (Figures 5D and S6E). Meanwhile, hepatic steatosis that was observed in the *cA-circSlc8a1*-transgenic mice was not seen in the double transgenic mice (Figures 5E and S6F).

To further verify the specific blocking of *circSlc8a1* by *cA-circSlc8a1*, we examined the levels of free *circSlc8a1* by introducing different amounts of *cA-circSlc8a1* into the HL-1 cells. Our results demonstrated that the levels of *circSlc8a1* were gradually decreased with transfection of elevated amounts of *cA-circSlc8a1* plasmids, detected by both circRNA-specific RT-qPCR (Figure 5F) and the RNA pull-down assay (Figure 5G). In addition, to exclude the possibility that the uncircularized linear *cA-circSlc8a1* precursor after transfection could also bind to and block *circSlc8a1*, we designed a construct with an intronic mutation which only generated linear *cA-circSlc8a1* precursor but not the circular form of *cA-circSlc8a1*. Our results showed that the linear *cA-circSlc8a1* precursor could not decrease the levels of unbound *circSlc8a1*, which indicated that only circularized *cA-circSlc8a1* could bind with *circSlc8a1* and block its function (Figures 5H and 5I). Taken together, these results demonstrated that the effects of *cA-circSlc8a1* on cardiac hypertrophy and hepatic steatosis were exerted by blocking the physiological functions of *circSlc8a1*.

Interaction of *circSlc8a1* with mitochondria-associated proteins

To further investigate the mechanism of the protective effects of *circSlc8a1*, we identified the proteins that bind with *circSlc8a1* using a *circSlc8a1* probe to precipitate the *circSlc8a1*-binding proteins followed by mass spectrometry analysis. The list showed that 36% of the total precipitated proteins were mitochondrial proteins, and 85% of these mitochondrial proteins were among the top 20 *circSlc8a1*-binding proteins based on the abundance in the heart tissues of the *circSlc8a1*-transgenic mice (Figure 6A; Table S1). To further confirm the results from the mass spectrometry analysis, we examined the subcellular localization of *circSlc8a1* in the heart tissues of the *circSlc8a1*-transgenic mice and in HL-1 cells transfected with *circSlc8a1*. The results showed that *circSlc8a1* levels were significantly higher in the mitochondria of the heart tissues of the *circSlc8a1*-transgenic mice (Figure 6B) and in the *circSlc8a1*-transfected HL-1 cells (Figure 6C) compared with the cytoplasm content lacking mitochondria. The purity of the mitochondria was confirmed by detecting the expression of GAPDH in the cytosol and mitochondrially encoded *Atp8* (MT-ATP8) in the mitochondria (Figures 6D and 6E). We also found co-localization of *circSlc8a1* with the mitochondrial

after transverse aortic constriction (TAC) surgery. n = 6; *p < 0.05, **p < 0.01. (F) The levels of *circSlc8a1* were retained at the similar levels as those in the sham group in the hearts of *circSlc8a1*(+)-transgenic mice 12 weeks post TAC surgery, while the levels of *circSlc8a1* in the litter-matched negative mice (circNeg) were significantly decreased at the same time point after TAC surgery. n = 15; **p < 0.01. (G) Representative photographs of Masson trichrome, Sirius red, and WGA staining showed that cardiac fibrosis and cardiac hypertrophy were induced by TAC surgery in the *circSlc8a1* negative (circNeg) mice. Such fibrosis and hypertrophy could be prevented in the transgenic mice overexpressing *circSlc8a1*. (H) The representative echocardiography of *circSlc8a1*-transgenic mice subjected to TAC surgery. (I and J) The *circSlc8a1*(+) mice subjected to TAC prevented the impairment of the heart function that was validated by (I) left ventricular ejection fraction (LVEF) and (J) left ventricular fractional shortening (LVFS). n = 10; **p < 0.01.

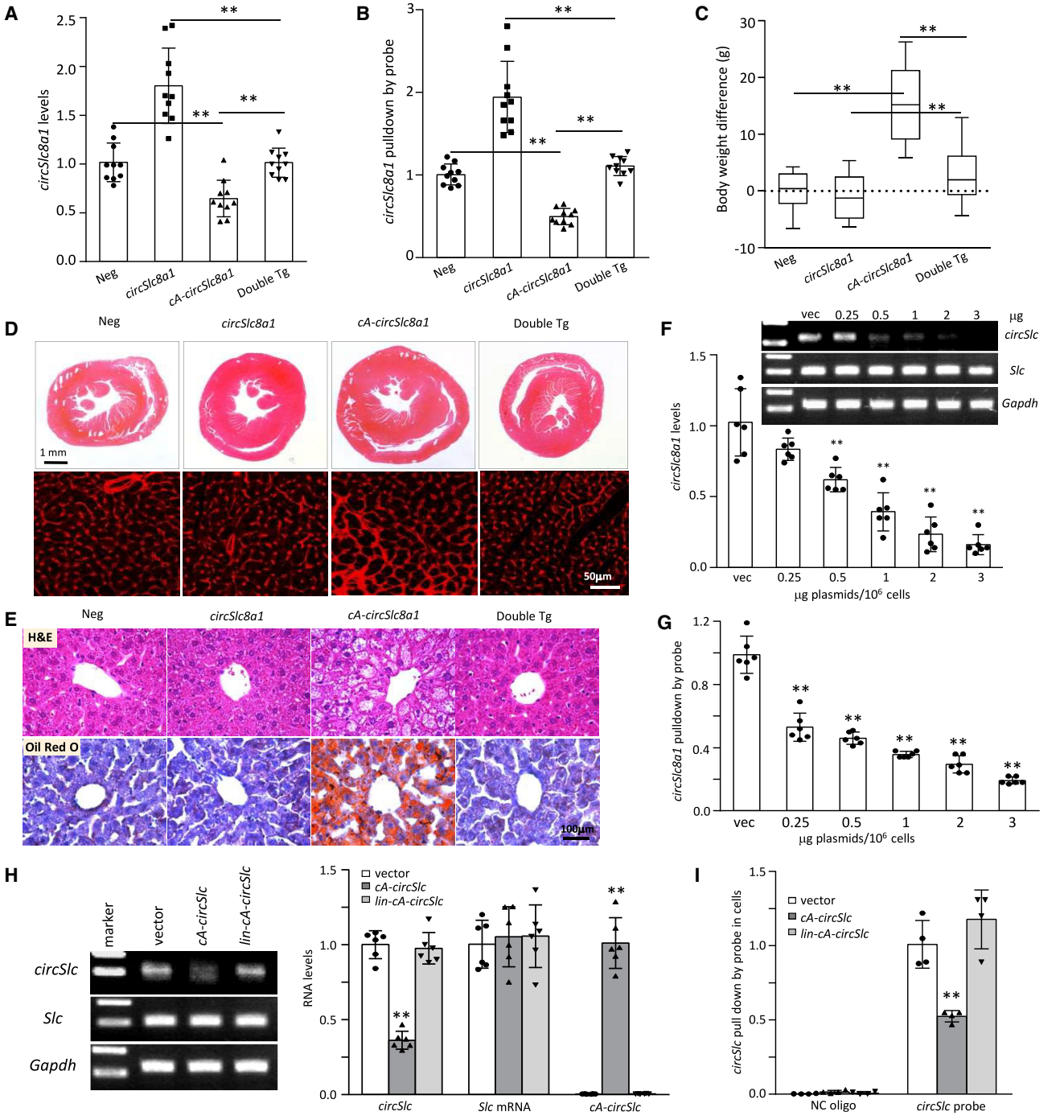

Figure 5. The rescue of phenotypic changes in *circSlc8a1* and *cA-circSlc8a1* double transgenic mice

(A) The levels of unbound *circSlc8a1* were detected by gene-specific RT-qPCR in *circSlc8a1*(+), *cA-circSlc8a1*(+), double transgenic mice, and the litter-matched negative mice. n = 10; **p < 0.01. (B) The levels of unbound *circSlc8a1* were detected by RNA pull-down assay with *circSlc8a1* probes in *circSlc8a1*(+), *cA-circSlc8a1*(+), double transgenic mice, and the litter-matched negative mice. n = 10; **p < 0.01. (C) The body weight difference in *circSlc8a1*(+), *cA-circSlc8a1*(+), double transgenic mice compared with the average of the litter-matched negative mice. n = 10; **p < 0.01. (D) Representative photographs of the whole hearts and WGA staining showed that cardiac hypertrophy was not induced in the double transgenic mice compared with the *cA-circSlc8a1*(+)-transgenic mice. n = 10. (E) Representative photographs of H&E and Oil Red O staining showed that hepatic steatosis was not induced in the double transgenic mice compared with the *cA-circSlc8a1*(+)-transgenic mice. n = 10. (F) The levels of unbound *circSlc8a1* were detected by gene-specific RT-qPCR after 0.25, 0.5, 1, 2, or 3 μg *cA-circSlc8a1* plasmids per 1 × 10^6 cells or the vectors were transfected. n = 6;

(legend continued on next page)

marker (VDAC) in the HL-1 cells (Figure 6F) and the heart tissues of the *cA-circSlc8a1*-transgenic mice (Figure 6G) using fluorescence *in situ* hybridization (FISH) and IHF staining, which suggested that *circSlc8a1* was translocated into the mitochondria to exert its function.

We further confirmed that *circSlc8a1* could bind with the proteins of ATP synthase subunit B (ATPB), cytochrome *c* oxidase (COX5B), NADH dehydrogenase iron sulfur protein 2 (NDUFS2), and mitochondria import receptor subunit TOMM22 in the heart tissues of the *circSlc8a1*-transgenic mice (Figures 7A and S7A) or the *cA-circSlc8a1*-transgenic mice (Figures 7B and S7B). Such binding was also validated in the cells transfected with *circSlc8a1* and *cA-circSlc8a1* plasmids (Figures 7C and S7C). In accordance, the interactions between *circSlc8a1* and the mitochondrial proteins, ATPB, COX5B, NDUFS2, and TOMM22, were also validated using the antibodies against these proteins to precipitate *circSlc8a1* in the transgenic heart tissues expressing *circSlc8a1* (Figure 7D) and cA-*circSlc8a1* (Figure 7E), and the HL-1 cells transfected with *circSlc8a1* and *cA-circSlc8a1* plasmids (Figure 7F). We also found that mitochondrial translocation of ATPB, COX5B, and NDUFS2 was facilitated by *circSlc8a1* and inhibited by *cA-circSlc8a1* using western immunoblotting (Figures 7G–7I and S7D–S7F). In addition, the *in situ* hybridization and immunofluorescence staining results also showed that the mitochondrial translocation of these proteins was significantly suppressed in the heart tissues of *cA-circSlc8a1*-transgenic mice compared with their negative litter (Figure S8). This indicated that *circSlc8a1* might be involved in the protein translocation to mitochondria via the translocase TOMM22 on the outer mitochondrial membrane. Since these mitochondrial proteins are associated with ATP generation in the mitochondria, we measured the ATP contents in the heart tissues of the *circSlc8a1*-transgenic mice and the *circSlc8a1*-transfected HL-1 cells. We observed a significant increase in ATP contents in the tissues and cells overexpressing *circSlc8a1*, which were reduced in the heart of *cA-circSlc8a1*-transgenic mice and *cA-circSlc8a1*-transfected cells (Figure 7J). These results suggested that *circSlc8a1* played its cardioprotective roles by promoting the protein translocation into the mitochondria and facilitating ATP production, which are essential to maintain heart function (Figure 7K).

DISCUSSION

Differential expression of circRNAs has been linked to different stages of myocardial development.[19] Dysregulation of circRNAs can lead to cardiovascular diseases, and may represent potential targets for therapeutics.[20,21] Usually, downregulated circRNAs could be compensated by ectopic delivery using nanoparticles or adeno-associated viruses.[22,23] However, knockdown of the upregulated circRNAs may also have off-target effects impacting the parental linear mRNA. To date, several approaches have attempted to silence circRNAs without removing the linear counterparts for *in vivo* functional studies. [5,14,15,24] In this study, we established a simple and effective method to knockdown cardiac circRNA *in vivo*, which may further be applied to circRNA functional studies and gene therapy in cardiovascular diseases.

Several antisense-based therapeutic methods for linear RNAs have been thoroughly investigated in preclinical studies and have been applied clinically.[25,26] The circRNAs possess unique structural conformations distinct from the linear RNA cognates,[27] therefore, we engineered circularized antisense RNA to only silence circRNA. The most beneficial aspect of using circular antisense RNA is that it could possibly be used for knocking down individual circRNA depending on its own sequence or structure. By forming a complementary circle against its sense counterpart, circular antisense RNA is specific for the target circRNA of interest and does not interfere with the linear mRNA cognate. In the present study, we used the circular antisense RNA of *circSlc8a1*, named *cA-circSlc8a1*, as an example to demonstrate the effects of circular antisense RNA on sequestering its sense circRNA. The circularized antisense RNA *cA-circSlc8a1* is complementary to *circSlc8a1* based on the oligonucleotide sequence, which suggests that *cA-circSlc8a1* and *circSlc8a1* may form a double-stranded RNA circle, at least partially. While the secondary structure might be a complex, the significant high affinity between *cA-circSlc8a1* and *circSlc8a1* was confirmed by the computational docking method. Notably, our results demonstrated that *cA-circSlc8a1* sequestered *circSlc8a1* without affecting the full-length linear *Slc8a1* mRNA cognate and its corresponding SLC8A1 protein in cardiomyocytes or heart tissues. One possible explanation could be that the unique circularized structure of *cA-circSlc8a1* rendered it less possible to bind to and sequester the linear *Slc8a1* mRNA.[27] We then established a transgenic animal model with *circSlc8a1* specifically silenced in the heart with *cA-circSlc8a1* driven by a heart promoter. By using *cA-circSlc8a1*, *circSlc8a1* functions in the heart were blocked. The cardiac-specific expression of *cA-circSlc8a1* in mice caused dramatic phenotypic changes, including significant increase in the body weight, hepatic steatosis, and impaired heart functions. Such phenotype changes provided evidence to demonstrate that circular antisense RNA could effectively sequester the function of the targeting circRNA. With this approach, we successfully established a mouse model for studying cardiac hepatopathy and demonstrated the essential roles of *circSlc8a1* in maintaining heart function. Consistent with this conclusion, another transgenic mouse model with overexpression of *circSlc8a1* validated the protective effects of *circSlc8a1* in a PO model. Previous studies reported that the levels of *circSlc8a1* were increased in the TAC or ischemia-reperfusion mouse models.[28,29]

**$p < 0.01$ versus vector. (G) The levels of unbound *circSlc8a1* were detected by the RNA pull-down assay with *circSlc8a1* probes after 0.25, 0.5, 1, 2, or 3 μg *cA-circSlc8a1* plasmids per 1×10^6 cells or the vectors were transfected. n = 6; **$p < 0.01$ versus vector. (H) The unbound *circSlc8a1* levels after transfection of vector, *cA-circSlc8a1* plasmids and the *cA-circSlc8a1* plasmids with mutated introns (lin-*cA-circSlc*). The levels of unbound *circSlc8a1* were detected by gene-specific RT-qPCR. n = 6; **$p < 0.01$ versus vector. (I) The unbound *circSlc8a1* levels were detected by the RNA pull-down assay after transfection with the vector, *cA-circSlc8a1* plasmids and the *cA-circSlc8a1* plasmids with mutated introns (lin-*cA-circSlc*). n = 6; **$p < 0.01$ versus vector.

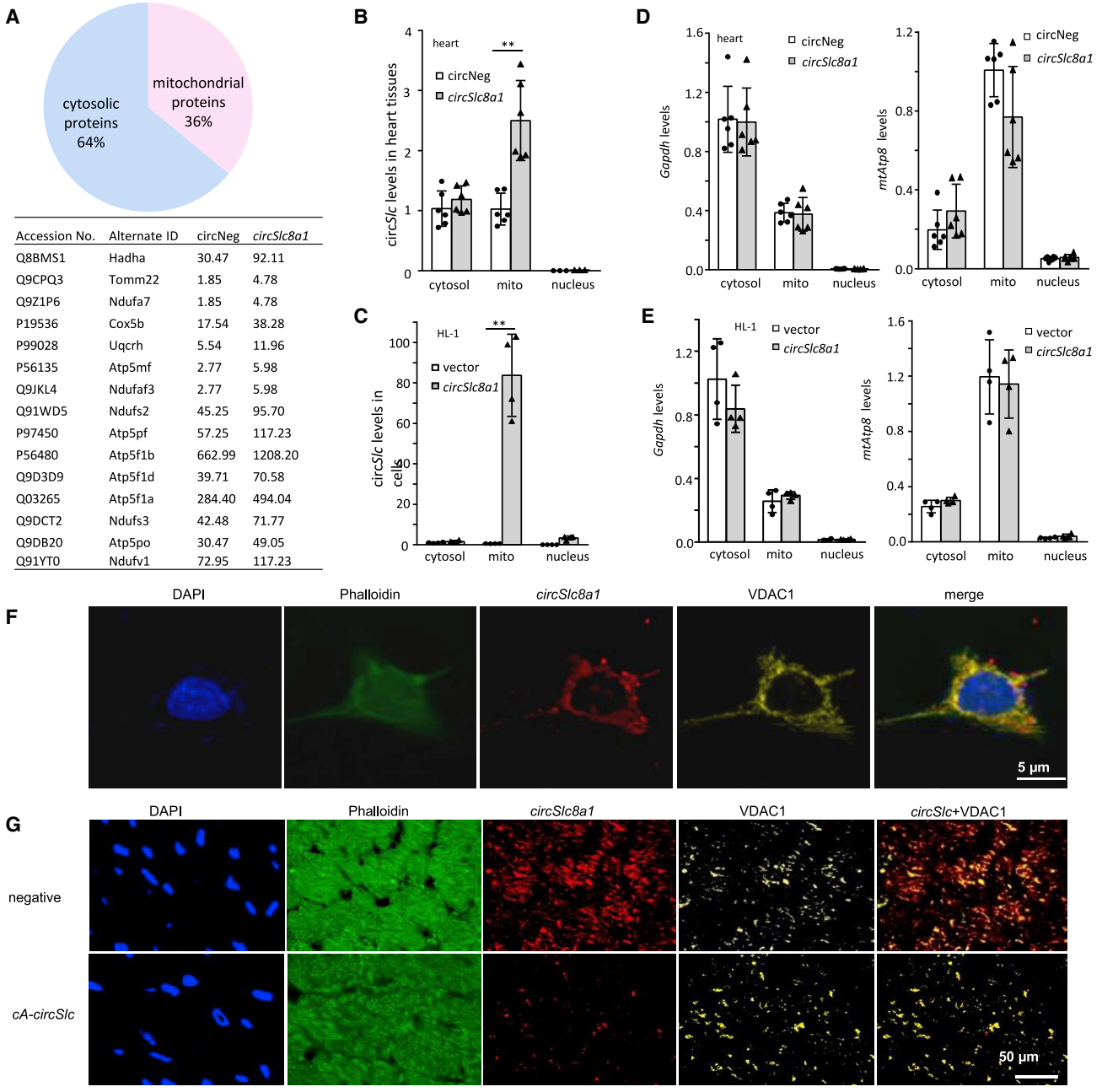

Accession No.	Alternate ID	circNeg	*circSlc8a1*
Q8BMS1	Hadha	30.47	92.11
Q9CPQ3	Tomm22	1.85	4.78
Q9Z1P6	Ndufa7	1.85	4.78
P19536	Cox5b	17.54	38.28
P99028	Uqcrh	5.54	11.96
P56135	Atp5mf	2.77	5.98
Q9JKL4	Ndufaf3	2.77	5.98
Q91WD5	Ndufs2	45.25	95.70
P97450	Atp5pf	57.25	117.23
P56480	Atp5f1b	662.99	1208.20
Q9D3D9	Atp5f1d	39.71	70.58
Q03265	Atp5f1a	284.40	494.04
Q9DCT2	Ndufs3	42.48	71.77
Q9DB20	Atp5po	30.47	49.05
Q91YT0	Ndufv1	72.95	117.23

Figure 6. *circSlc8a1* protected the heart function via binding to mitochondrial proteins

(A) Mass spectrophotometry analysis showed that 36% of the total proteins (types) precipitated by the *circSlc8a1* probe were mitochondrial proteins. (B) Subcellular localization of *circSlc8a1* in the cytosol (excluding mitochondria), mitochondria, and nuclei in the mouse heart tissues. n = 6; **p < 0.01 versus circNeg. (C) Subcellular localization of *circSlc8a1* in the cytosol (excluding mitochondria), mitochondria, and nuclei in HL-1 cells. n = 4; **p < 0.01 versus vector. (D) The purity of mitochondrial fraction in the mouse heart tissue was validated by examining *GAPDH* and the mitochondrially encoded *ATP8* (*MT-ATP8*). n = 5. (E) The purity of mitochondrial fraction in the HL-1 cells was validated by examining *GAPDH* and the mitochondriallly encoded *ATP8* (*MT-ATP8*). n = 5. (F) Representative photographs of the co-localization of *circSlc8a1* and the mitochondrial marker (VDAC) in HL-1 cells. (G) Representative photographs of the co-localization of *circSlc8a1* and the mitochondrial marker (VDAC) in negative and *cA-circSlc8a1*(+) mouse heart tissue.

In those studies, the levels of *circSlc8a1* were measured at 1 day or 3 weeks post-TAC. Our study showed that the levels of *circSlc8a1* at 2 weeks post-TAC were increased in the heart of TAC mice compared with the sham mice while they were reduced significantly 8–12 weeks post-TAC. Our results are consistent with the study from Lim et al., which showed that the endogenous levels of *circSlc8a1*

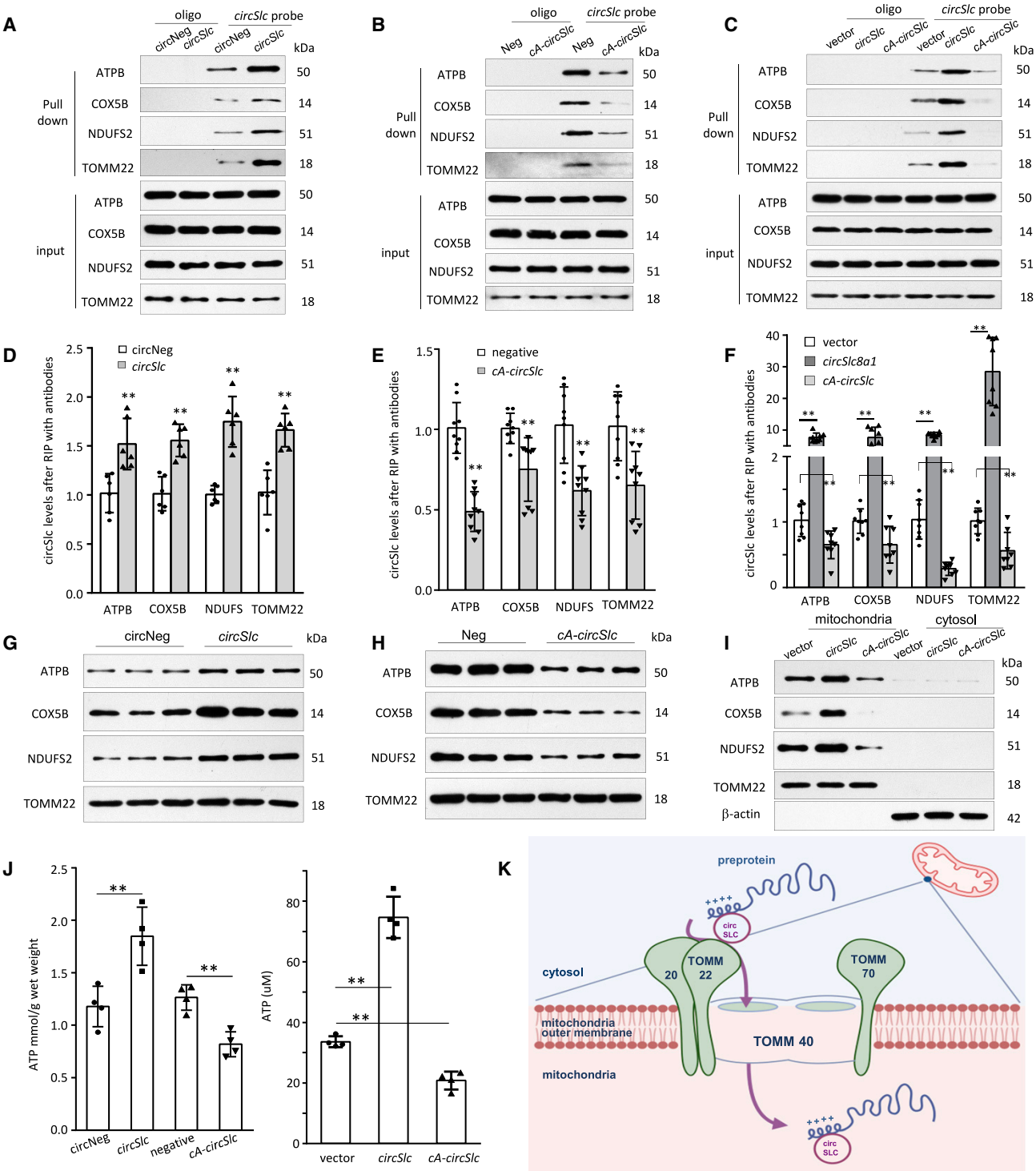

Figure 7. Interaction of *circSlc8a1* and the mitochondrial proteins

(A–C) Mitochondrial proteins ATPB, COX5B, NDUFS2, and TOMM22 were pulled down by *circSlc8a1* probe in the heart tissues of *circSlc8a1* (A) and *cA-circSlc8a1* (B) transgenic mice, and in HL-1 cells transfected with *circSlc8a1* or *cA-circSlc8a1* plasmids (C) followed by western blotting. n = 3–4. (D and E) Antibodies against ATPB, COX5B, NDUFS2, and TOMM22 were used to precipitate *circSlc8a1* from the heart tissues of *circSlc8a1* (D) and *cA-circSlc8a1* (E) transgenic mice. The immune-precipitated *circSlc8a1* was measured by qPCR. n = 6–9; **p < 0.01 versus negative mice. (F) *circSlc8a1* was immune-precipitated by ATPB, COX5B, NDUFS2, and

(legend continued on next page)

were decreased along with the impairment of the cardiac function in the hearts of TAC mice at 5 weeks post-TAC compared with the sham mice.[30] Taking the evidence together, we consider that *circSlc8a1* expression may increase at the early stage of PO to compensate for the acute impairment of ejection. However, cardiac fibrosis and heart failure occurred after long-term PO (8–12 weeks post-TAC), and ectopic expression of *circSlc8a1* could retain *cirSlc8a1* at physiological levels, which helped to protect heart function. Our study showed the strong dynamic effects of *circSlc8a1* during the progression of cardiac hypertrophy, cardiac remodeling, fibrosis, and heart failure.

Cardiac hepatopathy is associated with an increase of hepatic venous pressure and a decrease of portal vein inflow.[31] Over time, liver hypoperfusion and hepatic congestion lead to the development of thrombosis and an accumulation of deoxygenated blood in the liver resulting in hepatic steatosis and fibrosis.[32] Simonetto et al. developed a murine model of congestive hepatopathy by partial ligation of the inferior vena cava.[33] However, the congestive hepatopathy in this model was not directly derived from heart malfunction. In addition, previous studies have also shown that the heart plays important roles in systemic metabolic homeostasis. Deletion of MED13 protein or cardiac-specific miRNA, miR-208a, in the heart, led to body weight elevation and lipid accumulation in the liver.[34,35] Our study showed that genetic silencing of *circSlc8a1* by *cA-circSlc8a1* generated a model of heart failure leading to congestive hepatopathy. Knockdown of the cardiac *circSlc8a1* by its circularized antisense RNA led to an impaired heart function, a dramatic lipid accumulation in the liver and development of hepatic fibrosis/cirrhosis at the late stage. While providing a simple mouse model for defining the circRNA function, the present proof-of-conception study may also open a novel route for gene therapy targeting circRNA. Currently, two other circular antisense circRNAs designed with the same concept as *cA-circSlc8a1* are being employed for investigating circRNA functions in the heart based on their specific functions in the heart by sequestering their corresponding structures/functions in our laboratory. In our previous report, nanoparticle-conjugated plasmids were effectively delivered to the cardiac tissues and expressed well to produce circRNAs.[22] In the future, delivery of circularized anti-sense RNA has the potential to be used in gene therapy for the treatment of circRNA-related disorders.

Mechanistically, a large proportion of *circSlc8a1*-binding proteins were identified as mitochondrial proteins in mass spectrometry analysis, such as ATP synthase, cytochrome *c* oxidase, NADH dehydrogenase, and outer mitochondrial membrane protein TOMM22. Co-localized expression of *circSlc8a1* with mitochondrial markers in transfected cells and transgenic mice indicated that *circSlc8a1* might be translocated into the mitochondria after synthesis. Most of the mitochondrial proteins are encoded by nuclear genes and synthesized on cytosolic polysomes followed by translocation into the mitochondria via a protein sorting system.[36] These pre-proteins contain a consensus pre-sequence with mitochondrial targeting signal to be recognized by the mitochondrial import receptors TOMM20 and TOMM22 on the outer mitochondrial membrane.[37,38] Since *circSlc8a1* bound to a variety of mitochondrial proteins, we postulated that *circSlc8a1* might be able to recognize and bind with the mitochondrial targeting sequence of these nuclear-encoded mitochondrial proteins after the precursor proteins are synthesized in the cytosol. Meanwhile, *circSlc8a1* can also bind to TOMM22 on the outer membrane of mitochondria, which may facilitate these *circSlc8a1*-binding pre-proteins to interact with the outer membrane translocator complex and increase the import of these pre-proteins into the mitochondria (Figure 7K). By regulating these ATP generation-related enzymes, *circSlc8a1* played an essential role in maintaining heart function. However, the binding sites and the detailed transport mechanism need further investigation. In the previous studies of the circRNAs located in the mitochondria, the circRNAs were either generated by the mitochondrial genome[39] or co-localized with the mitochondrial proteins.[40,41] It is of great significance to identify how the nuclear genome-derived circRNAs were translocated into the mitochondria in the future studies.

In summary, we established a circRNA knockdown mouse model by using circular antisense RNA. It is a simple and more scalable method with broad general applicability to suppress the existential circRNAs *in vivo*. Sequestering *circSlc8a1* by its circular antisense RNA leads to malfunction of the heart, and subsequent cardiogenic hepatopathy. This *in vivo* circRNA knockdown model provides an effective strategy for circRNA functional studies and a potential approach for circRNA-related gene therapy.

MATERIALS AND METHODS

circRNA sequencing

The circRNA sequencing was conducted with the RNAs from the heart tissues obtained from 13 mice. The RNA samples were subjected to RNase R (ThemoFisher Scientific) treatment to degrade linear RNAs and depletion of rRNA. The remaining circRNAs were fragmented followed by RT using random primers. The circRNAs

TOMM22 antibodies in HL-1 cells transfected with *circSlc8a1* or *cA-circSlc8a1* plasmids followed by qPCR to detect the *circSlc8a1*. n = 6–9; **p < 0.01 versus vector. (G and H) Mitochondrial proteins were isolated from the heart tissue of *circSlc8a1* (G) and *cA-circSlc8a1* (H) transgenic mice. The mitochondrial translocation of ATPB, COX5B, and NDUFS2 proteins increased in the *circSlc8a1*-transgenic mice (G) but decreased in the *cA-circSlc8a1*-transgenic mice (H) compared with their counterpart negative litters. The outer mitochondrial membrane protein TOMM22 was not affected by *circSlc8a1* expression. n = 3–4. (I) The mitochondrial and the cytosolic proteins were separated from HL-1 cells transfected with *circSlc8a1* or *cA-circSlc8a1* plasmids. The mitochondrial translocation of ATPB, COX5B, and NDUFS2 proteins increased in the *circSlc8a1*-transfected cells but decreased in the *cA-circSlc8a1*-transfected cells compared with the vector controls. The purity of mitochondria and cytosol was confirmed by TOMM22 and β-actin antibodies. n = 3–4. (J) ATP levels were significantly increased by *circSlc8a1* overexpression and decreased by *cA-circSlc8a1* in the heart tissues of the transgenic mice (left) and HL-1 cells (right). n = 4; **p < 0.01. (K) A model depicting the proposed mechanism of *circSlc8a1* facilitating the translocation of pre-proteins from the cytosol into the mitochondria.

sequencing and analysis was performed by Novogene using Hi-Seq2500 System. The cDNA library was generated by the Novogene and then subjected to sequencing. Each circRNA was recorded by at least two reads spanning a head-to-tail splice junction in each sample.

Construct generation and primer design

The expression constructs of *cA-circSlc8a1* and *circSlc8a1* were generated according to the sequences shown in the supplemental information. The vector contains a Bluescript backbone, with one CMV promoter driving green fluorescent protein expression, and another CMV promoter driving the circRNA-forming fragments. For generating the cardiac-specific *cA-circSlc8a1*-transgenic mice, a heart promoter of mouse α-myosin heavy chain promoter cassette was inserted into *cA-circSlc8a1* construct according to the previous report.[42] For the vector control, *circSlc8a1* insert sequence was replaced with a non-related random sequence. The constructs of pre-*circSlc8a1* and pre-*cA-circSlc8a1* were generated in which the intronic sequences for circularization signal were mutated. Thus, pre-*circSlc8a1* and pre-*cA-circSlc8a1* would express their linear transcripts without circularization. The sequences for all the constructs and primers used are listed in the supplemental information.

Computational docking of *cA-circSlc8a1* with the circular and linear *Slc8a1*

To determine the secondary structures with lowest free energy, MFE algorithm implemented in Mfold (version 2.3) was used.[43] Mfold, a dynamic programming algorithm, uses energy minimization to model the ensemble of possible structures by identifying optimal folding of a nucleic acid sequence within a specified energy increment. The secondary structure with a lower theoretical value of free energy was selected as a model structure for 3D structure prediction. The output file containing primary sequence and an associated secondary structure (Dot-Bracket Notation) was then submitted to 3dRNA Web Server to generate the 3D structure.[44] 3dRNA is an automated method of building RNA 3D structures from sequences and secondary structures by using the smallest secondary elements. Docked models were generated using a bimolecular docking server PatchDock. The main physicochemical measure that relates to binding affinity is the buried surface area (BSA). BSA = (ASA antisense-circular RNA + ASA sense-circular RNA/linear mRNA) – ASA complex. Visualization was performed by using PyMOL.

Animal models

All animal experiments were conducted in accordance with the relevant guidelines and regulations approved by the Animal Care Committee of Sunnybrook Research Institute. The *cA-circSlc8a1* and *circSlc8a1*-transgenic mice were generated by pronuclear microinjection of DNA fragments containing either *cA-circSlc8a1* with the heart promoter or *circSlc8a1* into C57BL/6J, performed by the Toronto Centre for Phenogenomics. The sequences of cardiac-specific promoter (the promoter of mouse alpha myosin heavy chain gene) are shown in Figure S1E. The sequences of *cA-circSlc8a1* and *circSlc8a1* constructs for generating transgenic mice are listed in the supplemental information. All transgenic mice were ear tagged and genotyped after weaning. The genotyping primer sequences are listed in the Table S2.

PO-induced cardiac hypertrophy was performed by the modified TAC in mice as previously described.[45,46] Successful banding was confirmed with visual confirmation of differential carotid pulpability. Success in generating PO model was confirmed by measuring the carotid artery flow velocities by Doppler. Only mice with a right carotid/left carotid flow ratio within a certain range (>5) were included for further experiments. The sham mice underwent surgery at the same time points with anesthesia and the rest of the operation, except the aortic banding.

Cell culture and transfection

The immortalized mouse cardiomyocyte cell line, HL-1 cells, were cultured in Claycomb medium supplemented with 10% FBS, 100 U/mL penicillin and streptomycin, 2 mM L-glutamine and 0.1 mM norepinephrine. The HEK293 cells were cultured in DMEM supplemented with 10% FBS and 100 U/mL penicillin and streptomycin. The cells were transfected with the mixture of plasmid and transfection reagent Polyjet (SignaGen Laboratories) for 5–12 h and collected for further examination 24–48 h after transfection.

Cardiac function assessment

Mice were anesthetized with 2% isoflurane inhalation to undergo transthoracic echocardiography. Transthoracic echocardiography was performed and analyzed in a blinded manner, using a Vevo 2100 high-resolution imaging system equipped with a 40-MHz transducer to measure LVEDD, LVESD, LVEF, LVFS, and dp/dt. A 1.4-Fr high-fidelity pressure catheter (SPR-671, Millar Instruments, Houston, TX) was inserted into the LV via the right carotid artery to evaluate left ventricular pressure (LVSP) and dp/dt using PowerLab system (AD Instruments) as described.[47]

Histological staining

After harvesting, the hearts were cut into two halves. The lower halves were fixed with 10% buffered formalin and embedded in paraffin, sectioned into 5 μm sections. Masson's trichrome staining and Sirius red staining were performed to evaluate cardiac fibrosis. Masson's trichrome stain kit (American Master Tech) was used for Masson's trichrome staining according to the manufacturer's instructions. In brief, the paraffin sections were deparaffinized and hydrated with xylene and absolute alcohol followed by rinsing with running tap water. The sections were then immersed into preheated Bouin's Fluid at 56°C for 1 h followed by rinsing with running tap water until the tissues were colorless. Then, the sections were immersed in working Weigert's hematoxylin for 5 min, in Biebrich scarlet-acid fuchsin for 15 min, in phosphomolybdic/phosphotungstic acid for 15 min, in Aniline blue stain for 10 min, and then in 1% acetic acid for 5 min. The slides were rinsed with running tap water between each step. After dehydration, the slides were mounted with permanent mounting media.

The Sirius red staining was performed according to the protocol described in the previous report.[48] The mouse heart sections were de-waxed and hydrated, followed by staining with Weigert's haematoxylin for 8 min. The sections were washed with running tap water, stained in 0.1% Picrosirius red for 1 h, and then washed in 0.1% acetic acid. After dehydration, the slides were mounted with permanent mounting media.

WGA staining was conducted to visualize the cross-section area of cardiomyocytes for evaluating cardiac hypertrophy. Alexa Fluor 555 conjugated WGA (5 μg/mL) was applied to the tissue slides and incubated at room temperature for 10 min followed by washing twice with HBSS according to the manufacturer's instructions (ThermoFisher Scientific). Then, the slides were mounted with fluorescence mounting medium (Dako).

For ORO staining, the livers were fixed with 10% buffered formalin followed by immersion in 30% sucrose before embedded in OCT compound. Cryopreserved tissues were sectioned into 10 μm sections. The tissue slides were stained with ORO working solution (0.7%, w/v) followed by washing out the excess stain. The slides were mounted with aqueous mounting media, Glycerol Gelatin (Sigma).

The fibrosis area, cross-section area and lipid droplets area were quantified using ImageJ software.

RT-PCR and RNase treatment

Total RNAs were extracted from cells and tissues using TriRNA isolation kit (Geneaid) or TRIzol (ThermoFisher Scientific). Total RNAs were subjected to RNase R treatment to remove linear RNAs or directly used for RT to synthesize single-stranded cDNA. RNase treatment was conducted as described previously.[49,50] In brief, 1 μg RNase R (Epicentre) or RNase A (QIAGEN) was added in the mixture and incubated at 37°C for 15 min prior to RT. RNA (1 μg) was subjected to RT and quantitative PCR (qPCR) using LunaScript SuperMix and LunaqPCR master mix (New England Biolabs). The small nuclear RNA U6 or GAPDH were used as internal controls to calculate the relative levels of the RNAs of interest. For examining the copy number of *circSlc8a1*, cDNA was prepared as described above followed by droplet digital PCR (Bio-Rad) conducted at Genomics Core Facility, Sunnybrook Research Institute. For gene-specific RT using reverse primer specific for *circSlc8a1*, 1 μg RNA was reverse transcribed using iScript select cDNA synthesis kit (Bio-Rad) with reverse primer specific for *circSlc8a1* (5′-gtacaataagacttccaactgc-3′). The sequences of primers are listed in the supplemental information.

RNA pull-down assay

The RNA pull-down assay was performed using a biotin-labeled circRNA probe as described before.[49,51] In brief, the tissues or cells were lysed in co-IP buffer (20 mM Tris-HCl [pH 7.5], 150 mM NaCl, 0.1 mM EDTA, 0.5% NP40 and protease inhibitor cocktail) and incubated with biotinylated DNA probes against *circSlc8a1* at room temperature for 2 h. Streptavidin C1 magnetic beads (50 μL) from Invitrogen were added to each of the probe-containing reaction, and further incubated at room temperature for another 1 h. The beads were collected and washed extensively with co-IP buffer for five times. The circRNA *circSlc8a1* pulled down by the probe was analyzed by RT-PCR. The proteins that bound to *circSlc8a1* and pulled down by the probe were analyzed by western blotting or mass spectrometry. The biotin-oligomers for RNA pull-down of mouse *circSlc8a1* were synthesized by Eurofins Genomics.

Subcellular fractionation

The subcellular fractions of the heart tissues or the cells were isolated as described.[52] In brief, cultured cells or heart tissues were harvested and resuspended in 500 μL fractionation buffer (250 mM sucrose, 20 mM HEPES [pH 7.4], 10 mM KCl, 2 mM MgCl2, 1 mM EDTA, 1 mM EGTA, and protease inhibitor cocktail). Then, the cells were homogenized by 10 passages through a 25-G needle using a 1 mL syringe and incubated on ice for 30 min. The heart tissues were homogenized in fractionation buffer using a Dounce homogenizer on ice. The nuclear pellet was collected by centrifugation at 720 × *g* for 5 min. The supernatant was centrifuged again at 10,000 × *g* for 15 min. The pellet containing mitochondria was collected followed by further wash with fractionation buffer. The supernatant containing the cytosolic fraction was concentrated and purified with Millipore centrifugal filter units. The purity of the mitochondria was confirmed by detecting the expression of GAPDH or β-ACTIN in the cytosol and mitochondrially encoded ATP8 (MT-ATP8) in mitochondria.

FISH and immunofluorescent staining

In the FISH, cy5-labeled DNA oligo probes against *circSlc8a1* were generated by fluorescence PCR labeling kit (Biolynx). The labeled probes were heated at 95°C for 2 min and chilled on ice immediately to prevent reannealing. A scramble sequence was labeled in the same way and used as a negative control. The fixed samples were dehydrated by washing for approximately 1 min each in 70%, 95%, and 100% ethanol. The dehydrated samples were air-dried and pretreated with hybridization solution in 55°C for 30 min. The pre-hybridized slides were incubated with 50 nM fluorescence-labeled DNA probes in hybridization buffer at 55°C for 2 h followed by serial washes with saline sodium citrate buffers. After the samples were blocked with TBS containing 10% goat serum for 30 min, immunofluorescence staining with mitochondrial marker, VDAC antibody (Abcam) was performed with incubation at 4°C overnight followed by Alex Fluor 647 anti-rabbit antibody (ThermoFisher Scientific). F-actin was stained with Alexa Fluor 488 phalloidin (ThermoFisher Scientific) for 2 h at room temperature. DAPI was stained with NucBlue Fixed Cell ReadyProbes Reagent (ThermoFisher Scientific). Then, the slides were mounted with fluorescence mounting medium (Dako).

Western blotting

The protein expression levels were determined by western blotting as previously described.[53] In brief, proteins were isolated from tissues or cells using RIPA buffer. Proteins in the lysates were separated by sodium dodecyl sulfate-polyacrylamide gel electrophoresis. The separated proteins were transferred onto a nitrocellulose membrane in 1× Tris/glycine buffer containing 20% methanol at 80 V and 4°C for 2 h.

The membranes were blocked in TBST buffer containing 5% (w/v) non-fat dry milk powder for 1 h followed by incubation with primary antibodies at 4°C overnight. The membranes were then washed and incubated with secondary antibodies at room temperature for 2 h. After washing, the bound antibodies were visualized with an ECL detection kit (Millipore). The monoclonal antibodies against SLC8A1 and ATPB were from Abcam. The antibodies against COX5B, NDUFS2, and TOMM22 were from ABclonal. The same membranes were re-probed with rabbit anti-β-ACTIN monoclonal antibody (Proteintech) to confirm equal loading of proteins for each sample.

ATP assay

The ATP levels in the heart tissues or cultured cells were measured by ATP assay kit from Abcam according to the manufacturer's instructions. In brief, the cultured cells were resuspended and homogenized in ATP assay buffer followed by centrifugation at 13,000 × *g* at 4°C for 5 min. The supernatant was collected and deproteinized by using 1 M perchloric acid (PCA). The heart tissues were homogenized in ice-cold PCA with a Dounce homogenizer and kept on ice for 30–45 min. After centrifuging at 13,000 × *g* for 2 min at 4°C, the supernatant was neutralized to pH 6.5–8 with KOH. Then, the supernatant, which was collected after another centrifugation, and the ATP standard were applied for fluorometric assay with the ATP probe, ATP converter and Developer Mix that was provided in the assay kit.

Mass spectrometry analysis

The mouse heart tissues were lysed in the co-IP buffer and applied for RNA pull-down assay with *circSlc8a1* probe following the methods described above. The streptavidin magnetic beads were collected and washed extensively with the co-IP buffer followed by washing with PBS. The streptavidin magnetic beads were sent to SPARC Molecular Analysis Centre (The Hospital for Sick Children, Toronto) for elution, digestion and mass spectrometry analysis.

Statistical analysis

All experiments were performed in triplicates or more. The numerical data were subjected to Student's t test with non-parametric two-tailed unpaired Mann-Whitney test for two groups or one-way ANOVA for three or more groups using GraphPad Prism. The levels of significance were set at $^{*}p < 0.05$ and $^{**}p < 0.01$.

DATA AVAILABILITY

All data and material supporting the findings of this study are presented in the paper and/or the supplemental materials. Additional data are available from the corresponding author upon request.

SUPPLEMENTAL INFORMATION

Supplemental information can be found online at https://doi.org/10.1016/j.ymthe.2022.10.005.

ACKNOWLEDGEMENTS

This work was supported by a grant entitled "Regulation of ventricular remodeling by a circRNA *circSlc8a1*" from the Canadian Institutes of Health Research (PJT-166107) to B.B.Y.

AUTHOR CONTRIBUTIONS

B.B.Y. supervised the project. N.W. and B.B.Y. designed the experiments. N.W., F.L., W.Y., W.W.D., C.Z., J.L., S.M., K.Z., and E.E. performed the experiments and analyzed the data. F.M.A. performed computational analysis of circRNA interaction. N.W. and B.B.Y. wrote the paper.

DECLARATION OF INTERESTS

The authors declare no competing interests.Ethics approval
All animal experiments were conducted in accordance with the relevant guidelines and regulations approved by the Animal Care Committee of Sunnybrook Research Institute.

REFERENCES

1. Zhang, C., Huo, S.T., Wu, Z., Chen, L., Wen, C., Chen, H., Du, W.W., Wu, N., Guan, D., Lian, S., and Yang, B.B. (2020). Rapid development of targeting circRNAs in cardiovascular diseases. Mol. Ther. Nucleic Acids *21*, 568–576.
2. Schulte, C., Barwari, T., Joshi, A., Theofilatos, K., Zampetaki, A., Barallobre-Barreiro, J., Singh, B., Sörensen, N.A., Neumann, J.T., Zeller, T., et al. (2019). Comparative analysis of circulating noncoding RNAs versus protein biomarkers in the detection of myocardial injury. Circ. Res. *125*, 328–340.
3. Gupta, S.K., Garg, A., Bär, C., Chatterjee, S., Foinquinos, A., Milting, H., Streckfuß-Bömeke, K., Fiedler, J., and Thum, T. (2018). Quaking inhibits doxorubicin-mediated cardiotoxicity through regulation of cardiac circular RNA expression. Circ. Res. *122*, 246–254.
4. Du, W.W., Yang, W., Chen, Y., Wu, Z.K., Foster, F.S., Yang, Z., Li, X., and Yang, B.B. (2017). Foxo3 circular RNA promotes cardiac senescence by modulating multiple factors associated with stress and senescence responses. Eur. Heart J. *38*, 1402–1412.
5. Huang, S., Li, X., Zheng, H., Si, X., Li, B., Wei, G., Li, C., Chen, Y., Chen, Y., Liao, W., et al. (2019). Loss of super-enhancer-regulated circRNA nfix induces cardiac regeneration after myocardial infarction in adult mice. Circulation *139*, 2857–2876.
6. Shan, K., Liu, C., Liu, B.H., Chen, X., Dong, R., Liu, X., Zhang, Y.Y., Liu, B., Zhang, S.J., Wang, J.J., et al. (2017). Circular noncoding RNA HIPK3 mediates retinal vascular dysfunction in diabetes mellitus. Circulation *136*, 1629–1642.
7. Bei, Y., Yang, T., Wang, L., Holvoet, P., Das, S., Sluijter, J.P.G., Monteiro, M.C., Liu, Y., Zhou, Q., and Xiao, J. (2018). Circular RNAs as potential theranostics in the cardiovascular system. Mol. Ther. Nucleic Acids *13*, 407–418.
8. Yang, L., Han, B., Zhang, Z., Wang, S., Bai, Y., Zhang, Y., Tang, Y., Du, L., Xu, L., Wu, F., et al. (2020). Extracellular vesicle-mediated delivery of circular RNA SCMH1 promotes functional recovery in rodent and nonhuman primate ischemic stroke models. Circulation *142*, 556–574.
9. Misir, S., Wu, N., and Yang, B.B. (2022). Specific expression and functions of circular RNAs. Cell Death Differ. *29*, 481–491.
10. Huang, C.K., Kafert-Kasting, S., and Thum, T. (2020). Preclinical and clinical development of noncoding RNA therapeutics for cardiovascular disease. Circ. Res. *126*, 663–678.
11. Ylä-Herttuala, S., and Baker, A.H. (2017). Cardiovascular gene therapy: past, present, and future. Mol. Ther. *25*, 1095–1106.
12. Wu, N., Qadir, J., and Yang, B.B. (2022). CircRNA perspective: new strategies for RNA therapy. Trends Mol. Med. *28*, 343–344.
13. Memczak, S., Jens, M., Elefsinioti, A., Torti, F., Krueger, J., Rybak, A., Maier, L., Mackowiak, S.D., Gregersen, L.H., Munschauer, M., et al. (2013). Circular RNAs are a large class of animal RNAs with regulatory potency. Nature *495*, 333–338.
14. Piwecka, M., Glažar, P., Hernandez-Miranda, L.R., Memczak, S., Wolf, S.A., Rybak-Wolf, A., Filipchyk, A., Klironomos, F., Cerda Jara, C.A., Fenske, P., et al. (2017). Loss of a mammalian circular RNA locus causes miRNA deregulation and affects brain function. Science *357*, eaam8526.
15. Li, S., Li, X., Xue, W., Zhang, L., Yang, L.Z., Cao, S.M., Lei, Y.N., Liu, C.X., Guo, S.K., Shan, L., et al. (2021). Screening for functional circular RNAs using the CRISPR-Cas13 system. Nat. Methods *18*, 51–59.

16. Heumuller, A.W., Jones, A.N., Mourão, A., Klangwart, M., Shi, C., Wittig, I., Fischer, A., Muhly-Reinholz, M., Buchmann, G.K., Dieterich, C., et al. (2021). Locus-conserved circular RNA cZNF292 controls endothelial cell flow responses. Circ. Res. *130*, 67–79.

17. Chen, S., Huang, V., Xu, X., Livingstone, J., Soares, F., Jeon, J., Zeng, Y., Hua, J.T., Petricca, J., Guo, H., et al. (2019). Widespread and functional RNA circularization in localized prostate cancer. Cell *176*, 831–843.e22.

18. Pamudurti, N.R., Patop, I.L., Krishnamoorthy, A., Ashwal-Fluss, R., Bartok, O., and Kadener, S. (2020). An in vivo strategy for knockdown of circular RNAs. Cell Discov. *6*, 52.

19. Jakobi, T., Czaja-Hasse, L.F., Reinhardt, R., and Dieterich, C. (2016). Profiling and validation of the circular RNA repertoire in adult murine hearts. Genomics Proteomics Bioinformatics *14*, 216–223.

20. Aufiero, S., Reckman, Y.J., Pinto, Y.M., and Creemers, E.E. (2019). Circular RNAs open a new chapter in cardiovascular biology. Nat. Rev. Cardiol. *16*, 503–514.

21. Garikipati, V.N.S., Verma, S.K., Cheng, Z., Liang, D., Truongcao, M.M., Cimini, M., Yue, Y., Huang, G., Wang, C., Benedict, C., et al. (2020). Author Correction: circular RNA CircFndc3b modulates cardiac repair after myocardial infarction via FUS/VEGF-A axis. Nat. Commun. *11*, 2234.

22. Wu, N., Xu, J., Du, W.W., Li, X., Awan, F.M., Li, F., Misir, S., Eshaghi, E., Lyu, J., Zhou, L., et al. (2021). YAP circular RNA, circYap, attenuates cardiac fibrosis via binding with tropomyosin-4 and gamma-actin decreasing actin polymerization. Mol. Ther. *29*, 1138–1150.

23. Meganck, R.M., Borchardt, E.K., Castellanos Rivera, R.M., Scalabrino, M.L., Wilusz, J.E., Marzluff, W.F., and Asokan, A. (2018). Tissue-dependent expression and translation of circular RNAs with recombinant AAV vectors in vivo. Mol. Ther. Nucleic Acids *13*, 89–98.

24. Zhang, Y., Nguyen, T.M., Zhang, X.O., Wang, L., Phan, T., Clohessy, J.G., and Pandolfi, P.P. (2021). Optimized RNA-targeting CRISPR/Cas13d technology outperforms shRNA in identifying functional circRNAs. Genome Biol. *22*, 41.

25. Roberts, T.C., Langer, R., and Wood, M.J.A. (2020). Advances in oligonucleotide drug delivery. Nat. Rev. Drug Discov. *19*, 673–694.

26. Foinquinos, A., Batkai, S., Genschel, C., Viereck, J., Rump, S., Gyöngyösi, M., Traxler, D., Riesenhuber, M., Spannbauer, A., Lukovic, D., et al. (2020). Preclinical development of a miR-132 inhibitor for heart failure treatment. Nat. Commun. *11*, 633.

27. Liu, C.X., Li, X., Nan, F., Jiang, S., Gao, X., Guo, S.K., Xue, W., Cui, Y., Dong, K., Ding, H., et al. (2019). Structure and degradation of circular RNAs regulate PKR activation in innate immunity. Cell *177*, 865–880.e21.

28. Werfel, S., Nothjunge, S., Schwarzmayr, T., Strom, T.M., Meitinger, T., and Engelhardt, S. (2016). Characterization of circular RNAs in human, mouse and rat hearts. J. Mol. Cell. Cardiol. *98*, 103–107.

29. Li, M., Ding, W., Tariq, M.A., Chang, W., Zhang, X., Xu, W., Hou, L., Wang, Y., and Wang, J. (2018). A circular transcript of ncx1 gene mediates ischemic myocardial injury by targeting miR-133a-3p. Theranostics *8*, 5855–5869.

30. Lim, T.B., Aliwarga, E., Luu, T.D.A., Li, Y.P., Ng, S.L., Annadoray, L., Sian, S., Ackers-Johnson, M.A., and Foo, R.S.Y. (2019). Targeting the highly abundant circular RNA circSlc8a1 in cardiomyocytes attenuates pressure overload induced hypertrophy. Cardiovasc. Res. *115*, 1998–2007.

31. Samsky, M.D., Patel, C.B., DeWald, T.A., Smith, A.D., Felker, G.M., Rogers, J.G., and Hernandez, A.F. (2013). Cardiohepatic interactions in heart failure: an overview and clinical implications. J. Am. Coll. Cardiol. *61*, 2397–2405.

32. Møller, S., and Bernardi, M. (2013). Interactions of the heart and the liver. Eur. Heart J. *34*, 2804–2811.

33. Simonetto, D.A., Yang, H.y., Yin, M., de Assuncao, T.M., Kwon, J.H., Hilscher, M., Pan, S., Yang, L., Bi, Y., Beyder, A., et al. (2015). Chronic passive venous congestion drives hepatic fibrogenesis via sinusoidal thrombosis and mechanical forces. Hepatology *61*, 648–659.

34. Grueter, C.E., van Rooij, E., Johnson, B.A., DeLeon, S.M., Sutherland, L.B., Qi, X., Gautron, L., Elmquist, J.K., Bassel-Duby, R., and Olson, E.N. (2012). A cardiac microRNA governs systemic energy homeostasis by regulation of MED13. Cell *149*, 671–683.

35. Baskin, K.K., Bookout, A.L., and Olson, E.N. (2014). The heart-liver metabolic axis: defective communication exacerbates disease. EMBO Mol. Med. *6*, 436–438.

36. Vögtle, F.N., Wortelkamp, S., Zahedi, R.P., Becker, D., Leidhold, C., Gevaert, K., Kellermann, J., Voos, W., Sickmann, A., Pfanner, N., and Meisinger, C. (2009). Global analysis of the mitochondrial N-proteome identifies a processing peptidase critical for protein stability. Cell *139*, 428–439.

37. van Wilpe, S., Ryan, M.T., Hill, K., Maarse, A.C., Meisinger, C., Brix, J., Dekker, P.J., Moczko, M., Wagner, R., Meijer, M., et al. (1999). Tom22 is a multifunctional organizer of the mitochondrial preprotein translocase. Nature *401*, 485–489.

38. Pfanner, N. (2000). Protein sorting: recognizing mitochondrial presequences. Curr. Biol. *10*, R412–R415.

39. Zhao, Q., Liu, J., Deng, H., Ma, R., Liao, J.Y., Liang, H., Hu, J., Li, J., Guo, Z., Cai, J., et al. (2020). Targeting mitochondria-located circRNA SCAR alleviates NASH via reducing mROS output. Cell *183*, 76–93.e22.

40. Gong, W., Xu, J., Wang, Y., Min, Q., Chen, X., Zhang, W., Chen, J., and Zhan, Q. (2022). Nuclear genome-derived circular RNA circPUM1 localizes in mitochondria and regulates oxidative phosphorylation in esophageal squamous cell carcinoma. Signal Transduct. Target. Ther. *7*, 40.

41. Zheng, H., Huang, S., Wei, G., Sun, Y., Li, C., Si, X., Chen, Y., Tang, Z., Li, X., Chen, Y., et al. (2022). CircRNA Samd4 induces cardiac repair after myocardial infarction by blocking mitochondria-derived ROS output. Mol. Ther. https://doi.org/10.1016/j.ymthe.2022.06.016.

42. Sanbe, A., Gulick, J., Hanks, M.C., Liang, Q., Osinska, H., and Robbins, J. (2003). Reengineering inducible cardiac-specific transgenesis with an attenuated myosin heavy chain promoter. Circ. Res. *92*, 609–616.

43. Zuker, M. (2003). Mfold web server for nucleic acid folding and hybridization prediction. Nucleic Acids Res. *31*, 3406–3415.

44. Wang, J., Wang, J., Huang, Y., and Xiao, Y. (2019). 3dRNA v2. 0: an updated web server for RNA 3D structure prediction. Int. J. Mol. Sci. *20*, 4116.

45. Zhang, X., Javan, H., Li, L., Szucsik, A., Zhang, R., Deng, Y., and Selzman, C.H. (2013). A modified murine model for the study of reverse cardiac remodelling. Exp. Clin. Cardiol. *18*, e115–e117.

46. Du, W.W., Xu, J., Yang, W., Wu, N., Li, F., Zhou, L., Wang, S., Li, X., He, A.T., Du, K.Y., et al. (2021). A neuroligin isoform translated by circNlgn contributes to cardiac remodeling. Circ. Res. *129*, 568–582.

47. Xu, J., Du, W.W., Wu, N., Li, F., Li, X., Xie, Y., Wang, S., and Yang, B.B. (2022). The circular RNA circNlgnmediates doxorubicin-inducedcardiac remodeling and fibrosis. Mol. Ther. Nucleic Acids *28*, 175–189.

48. Zeng, Y., Du, W.W., Wu, Y., Yang, Z., Awan, F.M., Li, X., Yang, W., Zhang, C., Yang, Q., Yee, A., et al. (2017). A circular RNA binds to and activates AKT phosphorylation and nuclear localization reducing apoptosis and enhancing cardiac repair. Theranostics *7*, 3842–3855.

49. Wu, N., Yuan, Z., Du, K.Y., Fang, L., Lyu, J., Zhang, C., He, A., Eshaghi, E., Zeng, K., Ma, J., et al. (2019). Translation of yes-associated protein (YAP) was antagonized by its circular RNA via suppressing the assembly of the translation initiation machinery. Cell Death Differ. *26*, 2758–2773.

50. Du, W.W., Yang, W., Li, X., Fang, L., Wu, N., Li, F., Chen, Y., He, Q., Liu, E., Yang, Z., et al. (2020). The circular RNA circSKA3 binds integrin beta1 to induce invadopodium formation enhancing breast cancer invasion. Mol. Ther. *28*, 1287–1298.

51. Du, W.W., Li, X., Ma, J., Fang, L., Wu, N., Li, F., Dhaliwal, P., Yang, W., Yee, A.J., and Yang, B.B. (2022). Promotion of tumor progression by exosome transmission of circular RNA circSKA3. Mol. Ther. Nucleic Acids *27*, 276–292.

52. Frezza, C., Cipolat, S., and Scorrano, L. (2007). Organelle isolation: functional mitochondria from mouse liver, muscle and cultured fibroblasts. Nat. Protoc. *2*, 287–295.

53. Li, H., Chang, L., Du, W.W., Gupta, S., Khorshidi, A., Sefton, M., and Yang, B.B. (2014). Anti-microRNA-378a enhances wound healing process by upregulating integrin beta-3 and vimentin. Mol. Ther. *22*, 1839–1850.

YMTHE, Volume *31*

Supplemental Information

Silencing mouse circular RNA *circSlc8a1* by circular antisense *cA-circSlc8a1* induces cardiac hepatopathy

Nan Wu, Feiya Li, Weining Yang, William W. Du, Faryal Mehwish Awan, Chao Zhang, Juanjuan Lyu, Sema Misir, Kaixuan Zeng, Esra Eshaghi, and Burton B. Yang

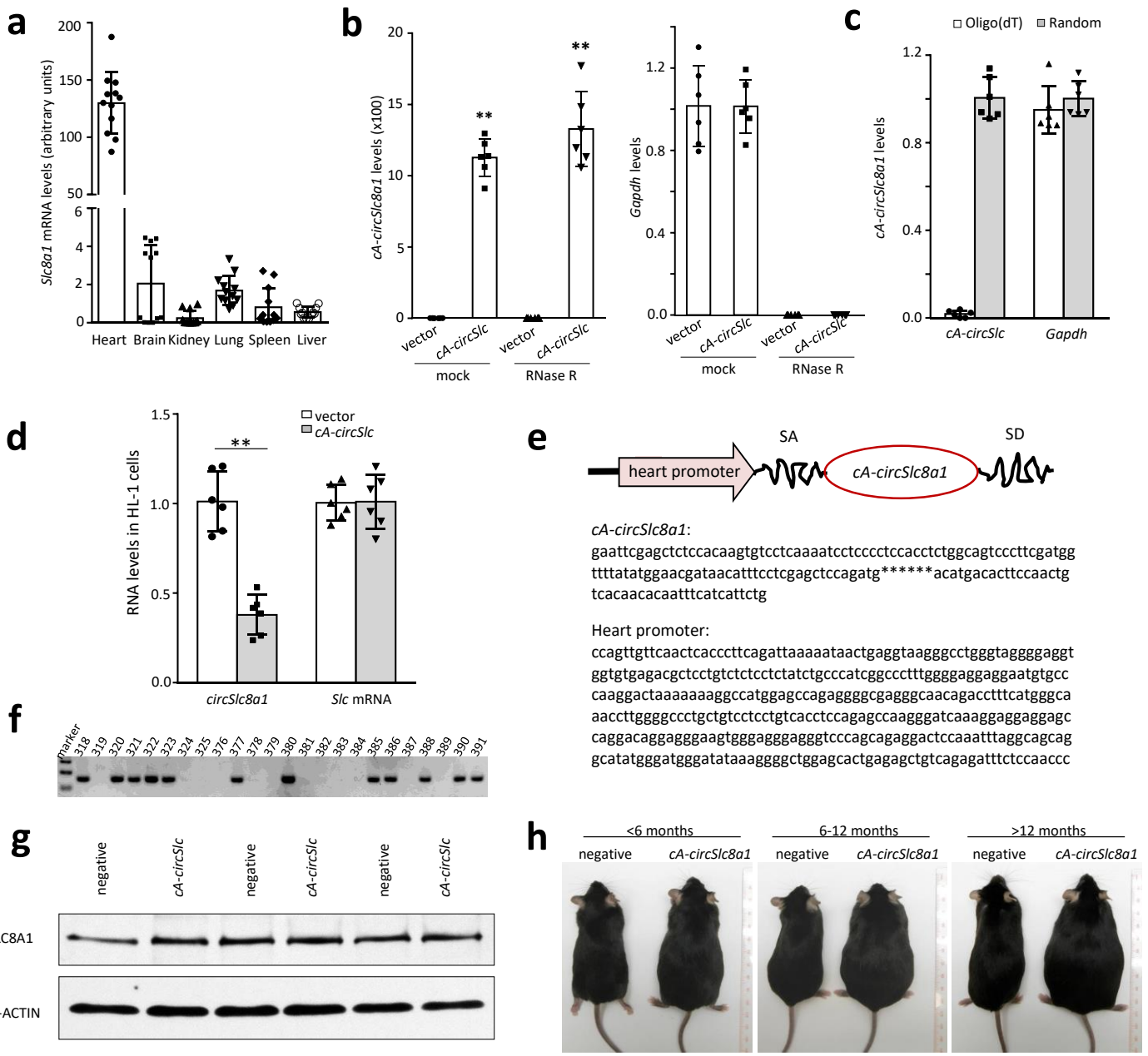

Supplementary Fig. S1. Generation of *circSlc8a1* knockdown mice by using circular antisense-*circSlc8a1* (*cA-circSlc8a1* or *cA-circSlc*) expression construct

(a) The expression levels of linear *Slc8a1* mRNA in different organs. n=12

(b) The *cA-circSlc8a1* construct was transfected into human HEK293T cells. The expression of *cA-circSlc8a1* (left) and *Slc8a1* mRNA (right) with or without RNase R treatment were determined by using mouse specific primers. n=6, **<0.01 vs vector control.

(c) The *cA-circSlc8a1* construct was transfected into human HEK293T cells. The RNAs from vector *or cA-circSlc8a1* transfected cells were reverse transcribed using random or oligo(dT) primers followed by qPCR using mouse specific primers. n=6, **<0.01 vs vector control.

(d) The levels of unbound *circSlc8a1* and *Slc8a1* mRNA in HL-1 cells transfected with *cA-circSlc8a1*. n=6, **<0.01 vs vector control.

(e) The construct were used to generate *cA-circSlc8a1* transgenic mice. The 5' and 3' sequences of *cA-circSlc8a1* and the heart promoter sequence are shown.

(f) Genotyping that validated the establishment of *cA-circSLC8A1* (+) transgenic mice.

(g) The levels of the SLC8A1 protein in the heart of *cA-circSlc8a1* transgenic mice.

(h) Representative photographs of *cA-circSlc8a1* (+) transgenic mice compared to the age-matched negative mice.

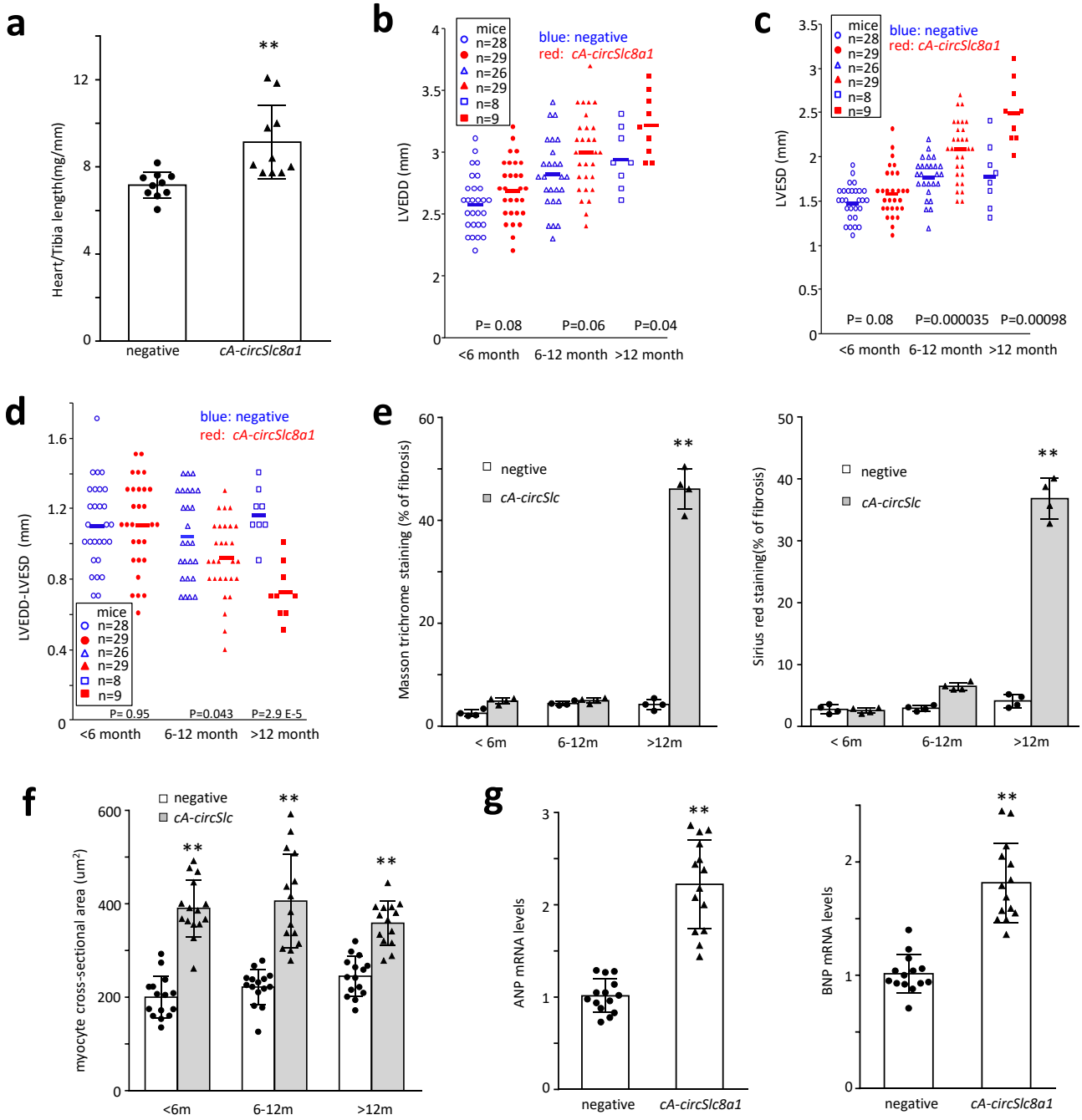

Supplementary Fig. S2. Analysis of heart function and fibrosis in the *cA-circSlc8a1* transgenic mice.

(a) The heart/tibia length ratio of *cA-circSlc8a1*(+) mice was significantly higher compared to litter match negative mice. n=10, ** p<0.01 vs negative.

(b) Echocardiography of *cA-circSlc8a1*(+) mice showed elevated left ventricular end-diastolic diameter (LVEDD) compared to litter match negative mice.

(c) Echocardiography of *cA-circSlc8a1*(+) mice showed elevated left ventricular end-systolic dimension (LVESD) compared to litter match negative mice.

(d) Echocardiography of *cA-circSlc8a1*(+) mice showed reduced LVEDD-LVESD compared to litter match negative mice.

(e) Quantification of fibrosis area observed by Masson trichrome staining (left), Sirius red staining (right). n=4, ** p<0.01 vs negative.

(f) Quantification of cross-section area of cardiomyocytes by WGA staining. n=15, ** p<0.01 vs negative.

(g) RNAs isolated from heart tissues of mice aged 6-12 month old were subjected to real-time qPCR to measure levels of ANP (left) and BNP (right). n=14, ** p<0.01.

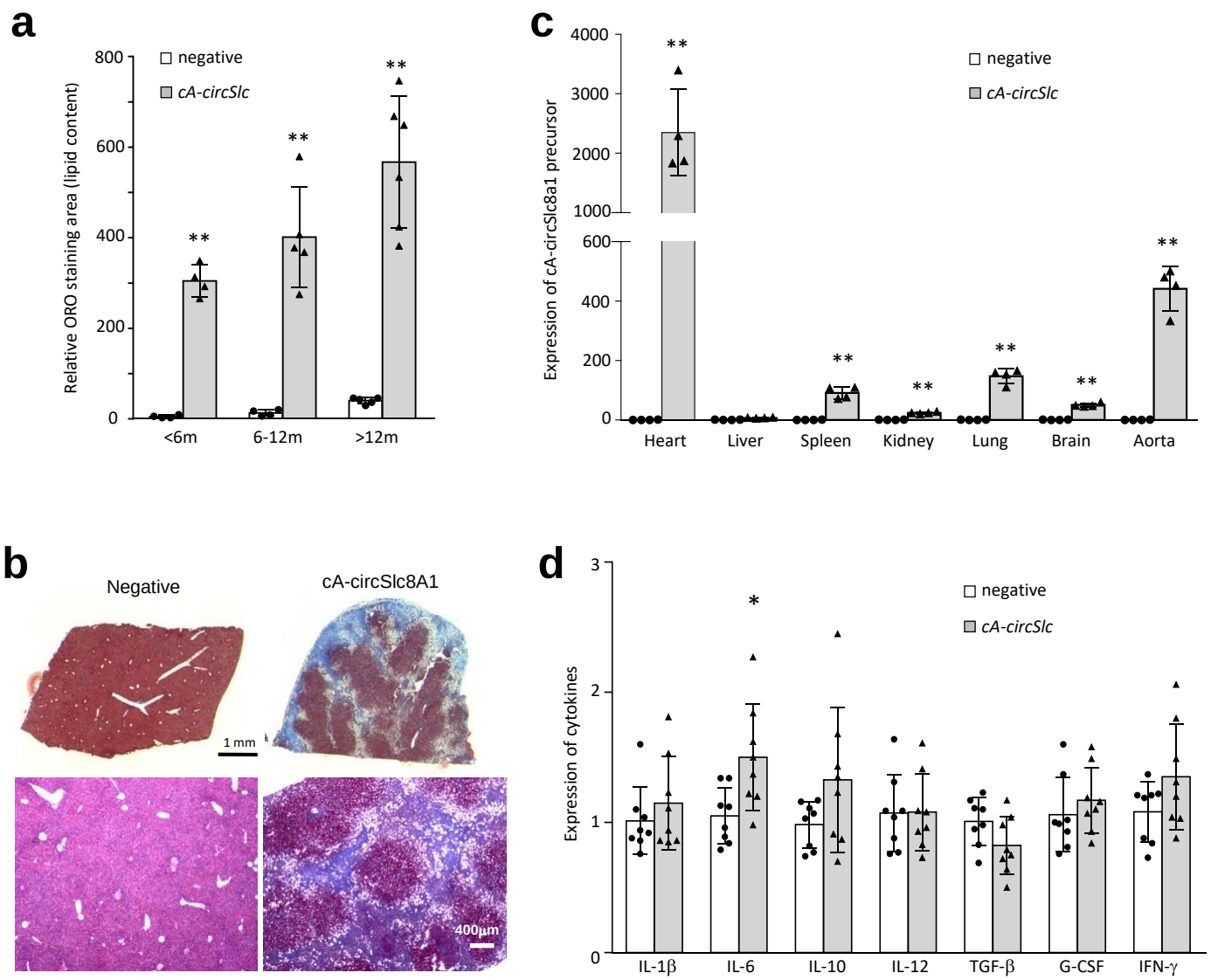

Supplementary Fig. S3. Transgenic mice with heart-specific expression of *cA-circSlc8a1* develop hepatic steatosis.

(a) Quantification of lipid content observed by Oil-Red-O staining. n=6, ** p<0.01 vs negative.

(b) Hepatic fibrosis/cirrhosis was developed in some of the *cA-circSlc8a1* mice (2 out of 14) at late stage, which examined by Masson trichrome staining.

(c) The expression of *cA-circSlc8a1* precursor in different organs. n=4, ** p<0.01 vs negative.

(d) The levels of cytokines measured by real-time PCR. * p<0.05 vs negative

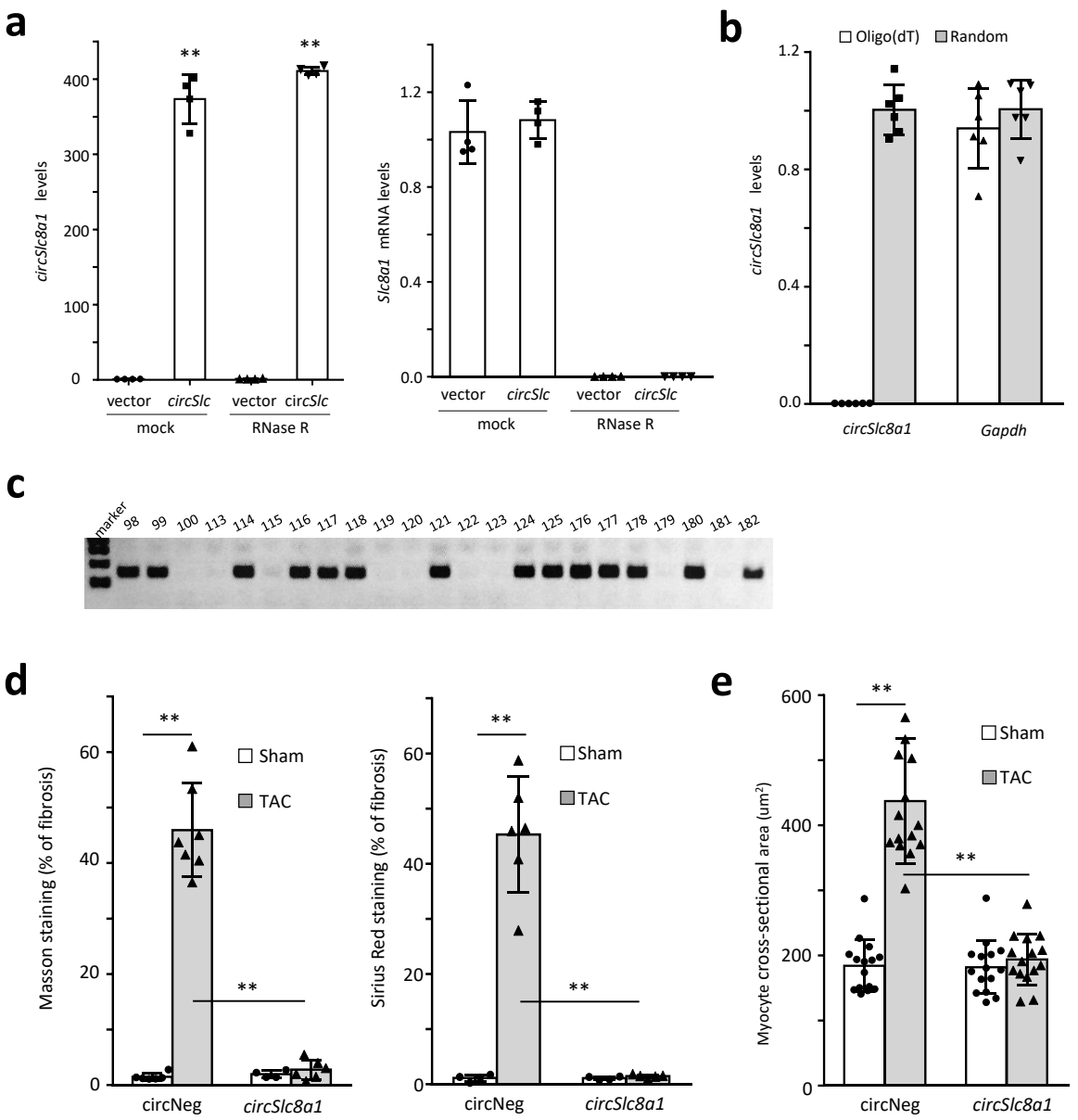

Supplementary Fig. S4. Generation of *circSlc8a1* transgenic mice and validation of the cardiac protective effects of *circSlc8a1*.

(a) The *circSlc8a1* constructs were transfected into human cell line HEK293T. The levels of *circSlc8a1* (left) and *Slc8a1* mRNA (right) with or without RNase R treatment were determined by using mouse specific primers respectively. n=4, **<0.01 vs vector control.

(b) The *circSlc8a1* constructs were transfected into human cell line HEK293T. The RNA were reverse transcribed by using random or oligo(dT) primers. The levels of *circSlc8a1* were determined by using mouse specific primers. n=6, **<0.01 vs vector control.

(c) Genotyping that validated the establishment of *circSlc8a1* (+) transgenic mice.

(d) Quantification of fibrosis area observed by Masson trichrome staining (left) and Sirius red staining (right). n=6, ** p<0.01

(e) Quantification of cross-section area of cardiomyocytes by WGA staining. n=15, ** p<0.01

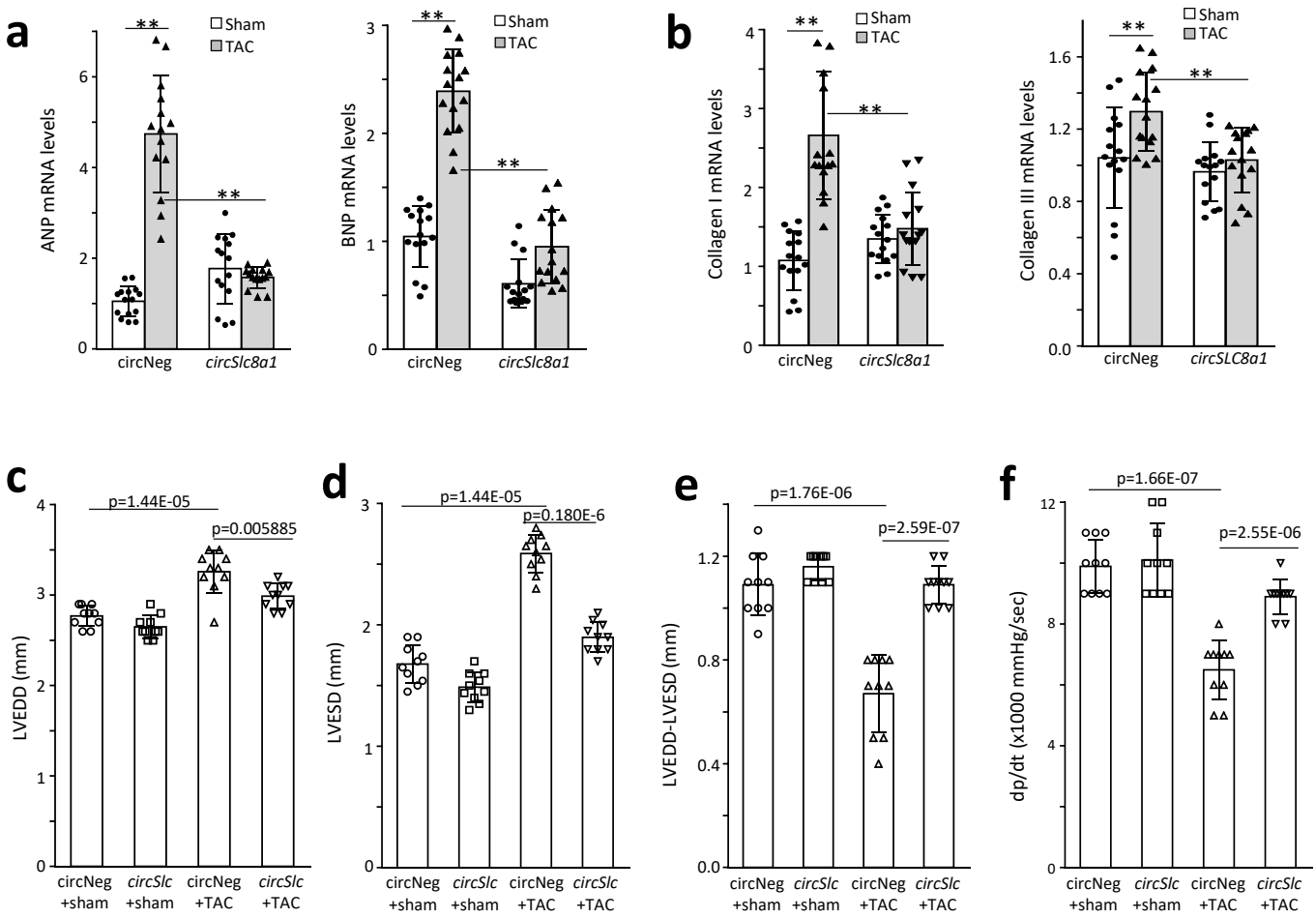

Supplementary Fig. S5. The *circSlc8a1* protect the heart from cardiac hypertrophy, cardiac fibrosis and impaired heart function.

(a) The levels of heart failure markers ANP (left) and BNP (right) were remarkably increased in the heart of negative mice by TAC surgery, while were significantly lower in the circSlc8a1 (+) mice compared to the litter match negative mice after TAC surgery. n=15, ** $p<0.01$.

(b) The levels of cardiac fibrosis markers collagen-I (left) and collagen-III (right) were remarkably increased in the heart of negative mice by TAC surgery, while were significantly lower in the circSlc8a1-transgenic mice compared to the litter match negative mice after TAC surgery. n=15, ** $p<0.01$.

(c-f) The circSlc8a1(+) mice subjected to TAC prevented the impair of heart function that validated by (c) LVEDD, (d) LVESD, (e) LVEDD-LVESD, and (f) left ventricular pressure (dp/dt). n=10

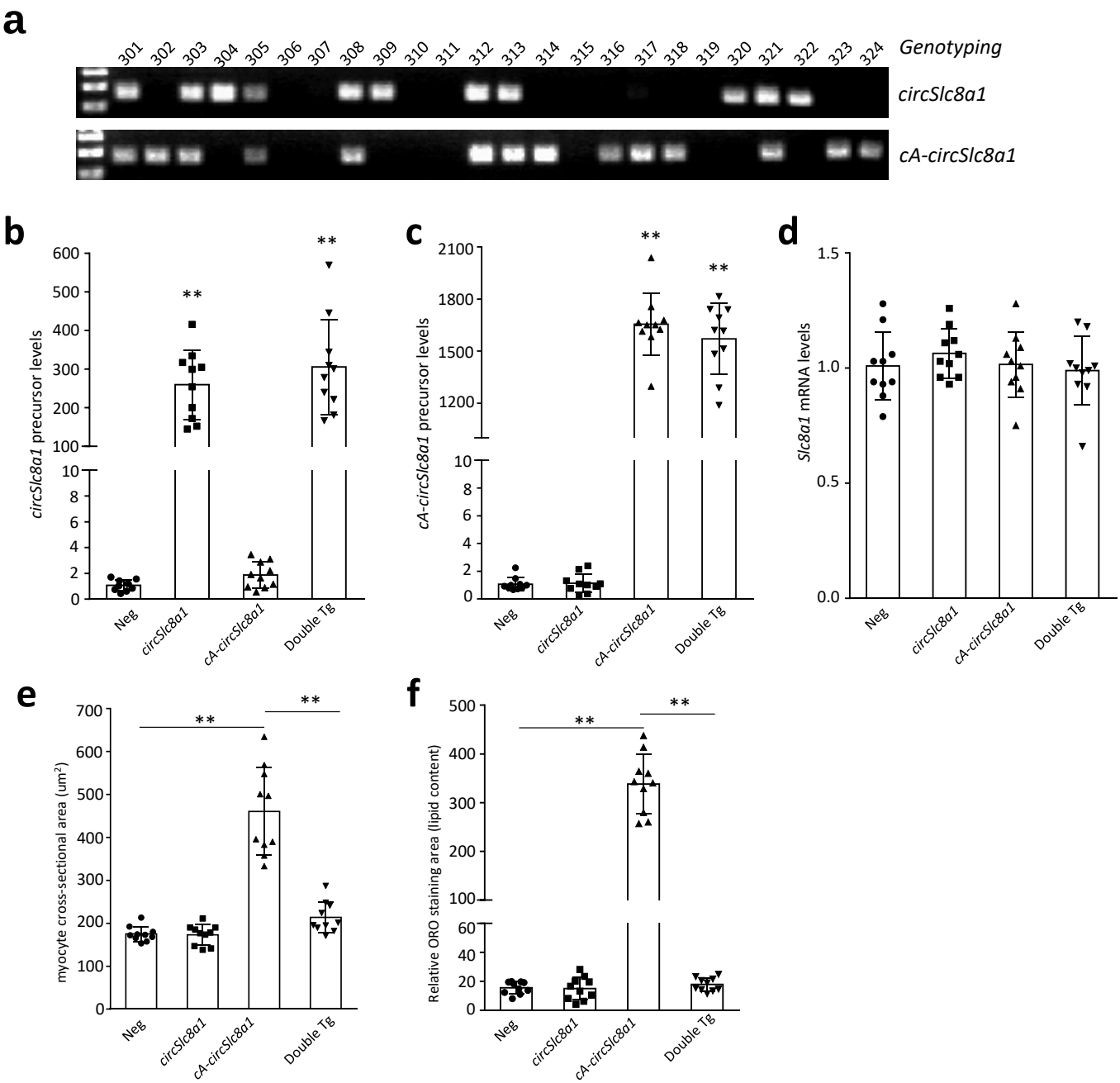

Supplementary Fig. S6. Generation of double transgenic mice with ectopic expression of both *circSlc8a1* and *cA-circSlc8a1*.

(a) Genotyping that validated the establishment of *circSlc8a1* (+) transgenic mice.

(b) The expression levels of *circSlc8a1* precursor in negative (Neg), *circSlc8a1* (+) transgenic mice, *cA-circSlc8a1* (+) transgenic mice, or double transgenic mice. n=10, **<0.01 vs negative mice.

(c) The expression levels of *cA-circSlc8a1* precursor in negative (Neg), c*circSlc8a1* (+) transgenic mice, *cA-circSlc8a1* (+) transgenic mice, or double transgenic mice. n=10, **<0.01 vs negative mice.

(d) The expression levels of *Slc8a1 mRNA* in negative (Neg), c*circSlc8a1* (+) transgenic mice, *cA-circSlc8a1* (+) transgenic mice, or double transgenic mice. n=10

(e) Quantification of cross-section area of cardiomyocytes by WGA staining. n=10, ** p<0.01

(f) Quantification of lipid content observed by Oil Red O. n=10, ** p<0.01

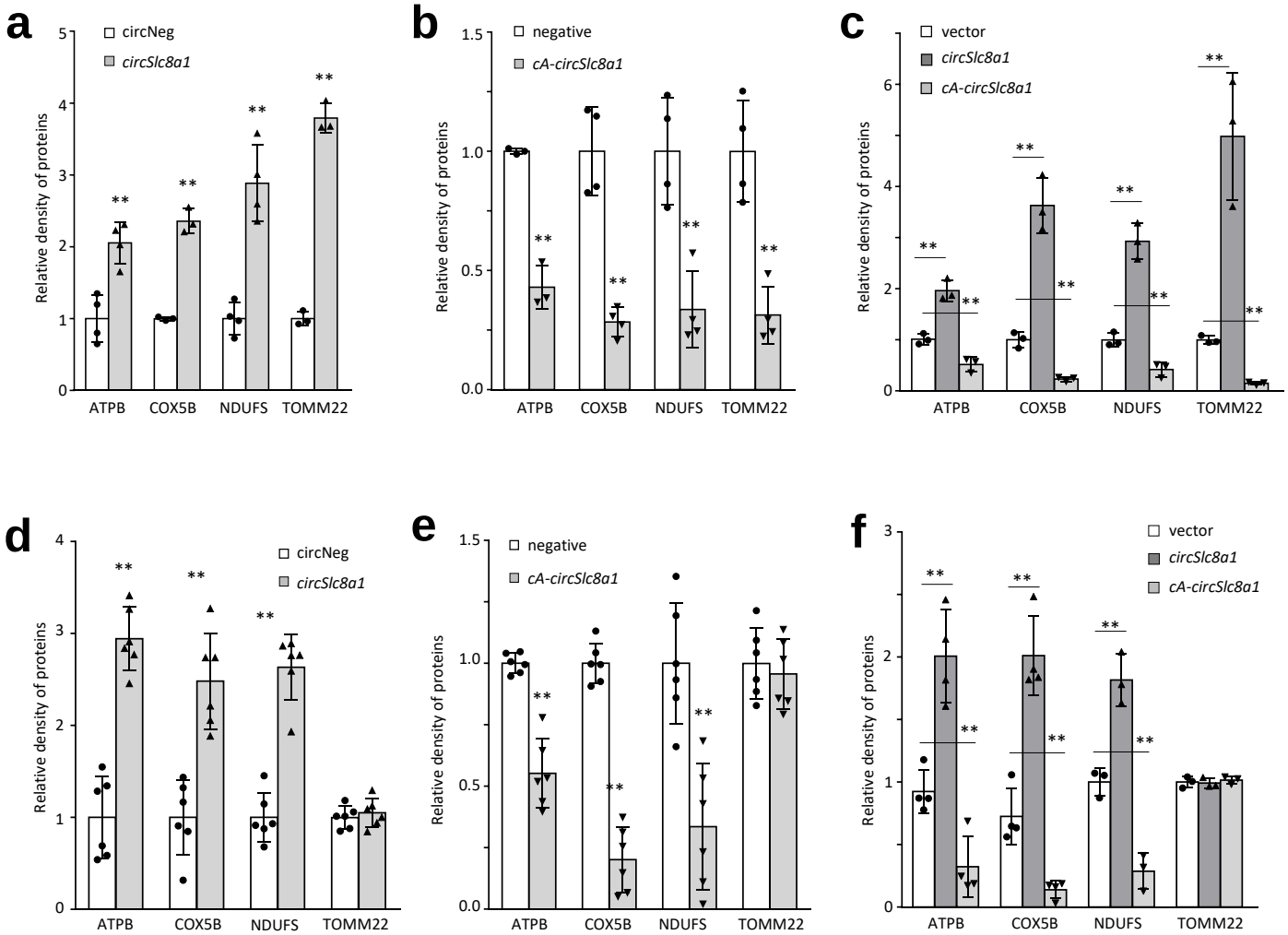

Supplementary Fig. S7. The *circSlc8a1* protected heart function via binding with mitochondrial proteins.

(a-c) The density of the bands in Western blot images presented in Fig.7a-c regarding the *circSlc8a1* pull down proteins was analysis. ** $p<0.01$, n=3-4

(d-f) The density of the bands in Western blot images presented in Fig.7d-f regarding the mitochondrial translocation of proteins was analysis. ** $p<0.01$, n=4-6

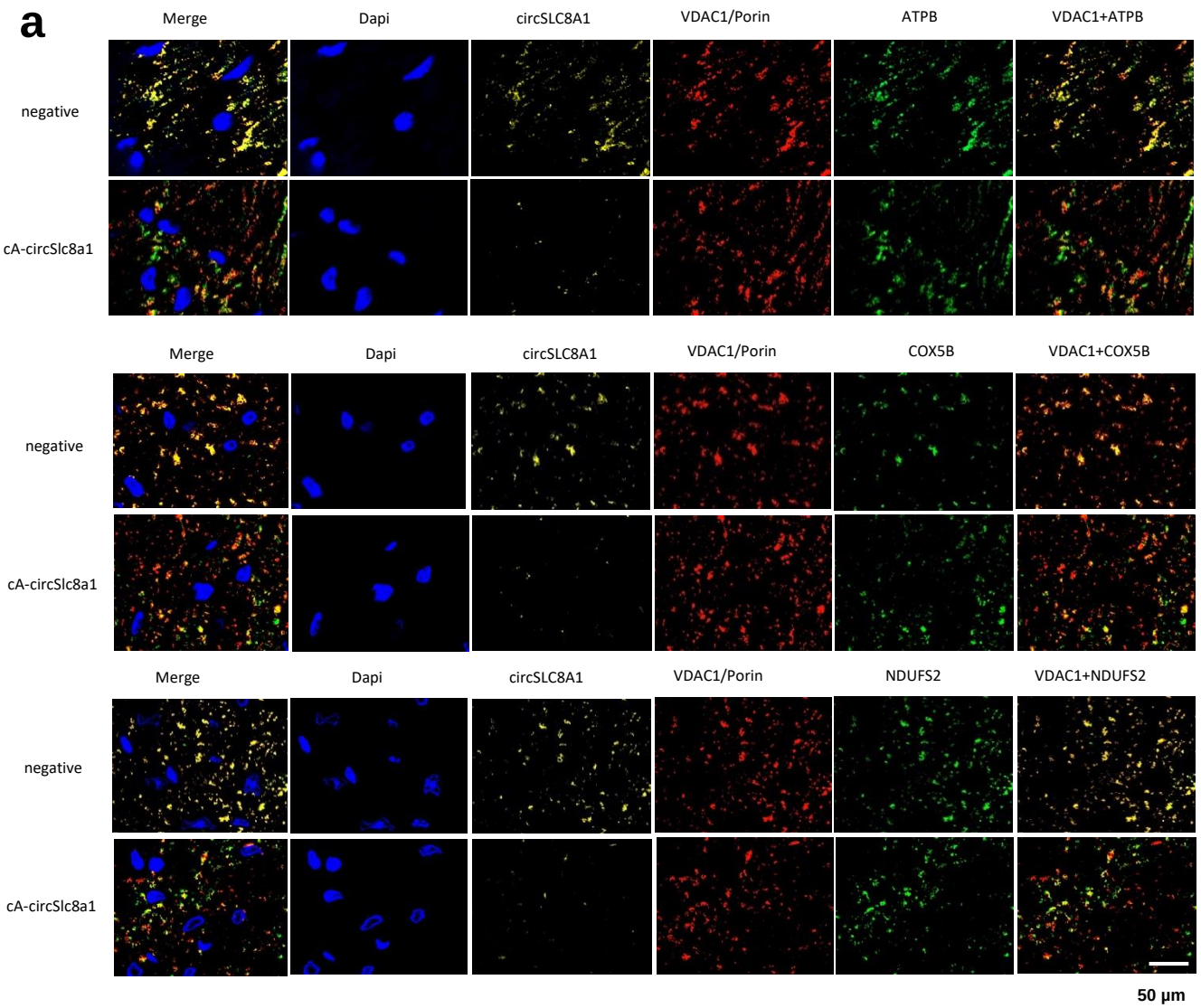

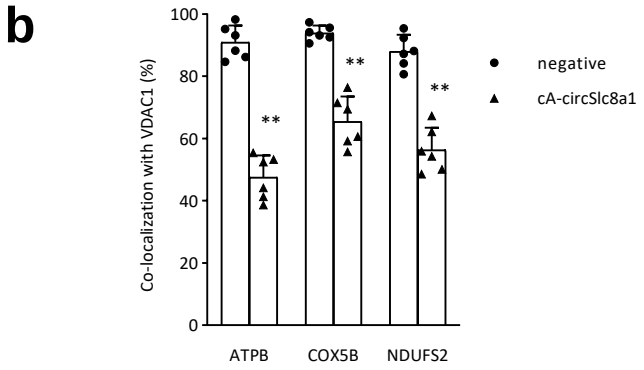

Supplementary Fig. S8. Co-localization of *circSlc8a1* with ATPB, COX5B, and NDUFS2.
Fig (a) In situ hybridization of *circSlc8a1* and immunofluorescence staining of ATPB, COX5B, and NDUFS2 in the *cA-circSlc8A1* transgenic and litter-matched negative mice. Representative photographs show co-localization of *circSlc8a1* with these mitochondrial proteins. (b) Quantitation of the staining. **, $p<0.01$.

Supplemetary Table 1: Protein identified by mass spectomatry analysis

#	Identified Proteins (750)	Accession Number	ID	Molecular Weight	circNeg	circSLC8A1	Fold change
1	ATP synthase subunit beta, mitochondrial OS=Mus musculus (Mouse) OX=10090 GN=Atp5f1b PE=1 SV=2	P56480	Atp5f1b	56 kDa	662.99	1,208.20	1.82
2	ATP synthase subunit alpha, mitochondrial OS=Mus musculus (Mouse) OX=10090 GN=Atp5f1a PE=1 SV=1	Q03265	Atp5f1a	60 kDa	284.4	494.04	1.74
3	Methylcrotonoyl-CoA carboxylase beta chain, mitochondrial OS=Mus musculus (Mouse) OX=10090 GN=Mccc2 PE=1 SV=1	Q3ULD5	Mccc2	61 kDa	204.99	284.7	1.39
4	NADH-ubiquinone oxidoreductase 75 kDa subunit, mitochondrial OS=Mus musculus (Mouse) OX=10090 GN=Ndufs1 PE=1 SV=2	Q91VD9	Ndufs1	80 kDa	164.36	261.97	1.59
5	ATP synthase subunit d, mitochondrial OS=Mus musculus (Mouse) OX=10090 GN=Atp5pd PE=1 SV=3	Q9DCX2	Atp5pd	19 kDa	83.105	131.58	1.58
6	ATP synthase-coupling factor 6, mitochondrial OS=Mus musculus (Mouse) OX=10090 GN=Atp5pf PE=1 SV=1	P97450	Atp5pf	12 kDa	57.25	117.23	2.05
7	NADH dehydrogenase [ubiquinone] flavoprotein 1, mitochondrial OS=Mus musculus (Mouse) OX=10090 GN=Ndufv1 PE=1 SV=1	Q91YT0	Ndufv1	51 kDa	72.948	117.23	1.61
8	Alpha-actinin-2 OS=Mus musculus (Mouse) OX=10090 GN=Actn2 PE=1 SV=2	Q9JI91	Actn2	104 kDa	87.722	114.84	1.31
9	Succinate dehydrogenase [ubiquinone] flavoprotein subunit, mitochondrial OS=Mus musculus (Mouse) OX=10090 GN=Sdha PE=1 SV=1	Q8K2B3	Sdha	73 kDa	65.561	96.894	1.48
10	NADH dehydrogenase [ubiquinone] iron-sulfur protein 2, mitochondrial OS=Mus musculus (Mouse) OX=10090 GN=Ndufs2 PE=1 SV=1	Q91WD5	Ndufs2	53 kDa	45.246	95.698	2.12
11	Trifunctional enzyme subunit alpha, mitochondrial OS=Mus musculus (Mouse) OX=10090 GN=Hadha PE=1 SV=1	Q8BMS1	Hadha	83 kDa	30.472	92.109	3.02
12	Propionyl-CoA carboxylase alpha chain, mitochondrial OS=Mus musculus (Mouse) OX=10090 GN=Pcca PE=1 SV=2	Q91ZA3	Pcca	80 kDa	55.403	88.521	1.60
13	Caveolae-associated protein 2 OS=Mus musculus (Mouse) OX=10090 GN=Cavin2 PE=1 SV=3	Q63918	Cavin2	47 kDa	63.714	86.128	1.35
14	NADH dehydrogenase [ubiquinone] iron-sulfur protein 3, mitochondrial OS=Mus musculus (Mouse) OX=10090 GN=Ndufs3 PE=1 SV=2	Q9DCT2	Ndufs3	30 kDa	42.476	71.774	1.69
15	ATP synthase subunit delta, mitochondrial OS=Mus musculus (Mouse) OX=10090 GN=Atp5f1d PE=1 SV=1	Q9D3D9	Atp5f1d	18 kDa	39.706	70.577	1.78
16	NADH dehydrogenase [ubiquinone] flavoprotein 2, mitochondrial OS=Mus musculus (Mouse) OX=10090 GN=Ndufv2 PE=1 SV=2	Q9D6J6	Ndufv2	27 kDa	48.016	69.381	1.44
17	IF rod domain-containing protein OS=Mus musculus (Mouse) OX=10090 GN=Krt83 PE=1 SV=1	E9Q1Y9	Krt83	53 kDa	0	52.634	
18	NADH dehydrogenase [ubiquinone] iron-sulfur protein 6, mitochondrial OS=Mus musculus (Mouse) OX=10090 GN=Ndufs6 PE=1 SV=2	P52503	Ndufs6	13 kDa	35.089	52.634	1.50
19	Trifunctional enzyme subunit beta, mitochondrial OS=Mus musculus (Mouse) OX=10090 GN=Hadhb PE=1 SV=1	Q99JY0	Hadhb	51 kDa	17.544	50.241	2.86
20	ATP synthase subunit O, mitochondrial OS=Mus musculus (Mouse) OX=10090 GN=Atp5po PE=1 SV=1	Q9DB20	Atp5po	23 kDa	30.472	49.045	1.61
21	Alpha-crystallin B chain OS=Mus musculus (Mouse) OX=10090 GN=Cryab PE=1 SV=2	P23927	Cryab	20 kDa	30.472	47.849	1.57
22	Coatomer subunit epsilon OS=Mus musculus (Mouse) OX=10090 GN=Cope PE=1 SV=3	O89079	Cope	35 kDa	22.161	46.653	2.11
23	NADH dehydrogenase [ubiquinone] iron-sulfur protein 8, mitochondrial OS=Mus musculus (Mouse) OX=10090 GN=Ndufs8 PE=1 SV=1	Q8K3J1	Ndufs8	24 kDa	29.549	46.653	1.58
24	Methylcrotonoyl-CoA carboxylase subunit alpha, mitochondrial OS=Mus musculus (Mouse) OX=10090 GN=Mccc1 PE=1 SV=2	Q99MR8	Mccc1	79 kDa	30.472	46.653	1.53
25	Lipoamide acyltransferase component of branched-chain alpha-keto acid dehydrogenase complex, mitochondrial OS=Mus musculus (Mouse) OX=10090 GN=Dbt PE=1	P53395	Dbt	53 kDa	31.395	43.064	1.37
26	Casein kinase II subunit beta OS=Mus musculus (Mouse) OX=10090 GN=Csnk2b PE=1 SV=1	P67871	Csnk2b	25 kDa	24.932	39.475	1.58
27	Cytochrome c oxidase subunit 5B, mitochondrial OS=Mus musculus (Mouse) OX=10090 GN=Cox5b PE=1 SV=1	P19536	Cox5b	14 kDa	17.544	38.279	2.18
28	Casein kinase II subunit alpha OS=Mus musculus (Mouse) OX=10090 GN=Csnk2a1 PE=1 SV=2	Q60737	Csnk2a1	45 kDa	21.238	38.279	1.80
29	Serine beta-lactamase-like protein LACTB, mitochondrial OS=Mus musculus (Mouse) OX=10090 GN=Lactb PE=1 SV=1	Q9EP89	Lactb	61 kDa	19.391	28.709	1.48
30	Histone H4 OS=Mus musculus (Mouse) OX=10090 GN=H4f16 PE=1 SV=2	P62806	H4f16	11 kDa	19.391	27.513	1.42
31	ATP synthase subunit gamma, mitochondrial OS=Mus musculus (Mouse) OX=10090 GN=Atp5f1c PE=1 SV=1	Q91VR2	Atp5f1c	33 kDa	17.544	25.121	1.43
32	Transcriptional activator protein Pur-alpha OS=Mus musculus (Mouse) OX=10090 GN=Pura PE=1 SV=1	P42669	Pura	35 kDa	10.157	22.728	2.24
33	RNA-binding motif protein, X chromosome OS=Mus musculus (Mouse) OX=10090 GN=Rbmx PE=1 SV=1	Q9WV02	Rbmx	42 kDa	14.774	21.532	1.46
34	2-oxoisovalerate dehydrogenase subunit alpha, mitochondrial OS=Mus musculus (Mouse) OX=10090 GN=Bckdha PE=1 SV=1	P50136	Bckdha	50 kDa	16.621	21.532	1.30
35	Pentatricopeptide repeat domain-containing protein 3, mitochondrial OS=Mus musculus (Mouse) OX=10090 GN=Ptcd3 PE=1 SV=2	Q14C51	Ptcd3	78 kDa	16.621	21.532	1.30
36	NADH dehydrogenase [ubiquinone] 1 alpha subcomplex subunit 5 OS=Mus musculus (Mouse) OX=10090 GN=Ndufa5 PE=1 SV=3	Q9CPP6	Ndufa5	13 kDa	12.927	20.336	1.57
37	Adenylate kinase isoenzyme 1 OS=Mus musculus (Mouse) OX=10090 GN=Ak1 PE=1 SV=1	Q9R0Y5	Ak1	22 kDa	12.927	19.14	1.48
38	28S ribosomal protein S22, mitochondrial OS=Mus musculus (Mouse) OX=10090 GN=Mrps22 PE=1 SV=1	Q9CXW2	Mrps22	41 kDa	14.774	19.14	1.30
39	Acyl-CoA dehydrogenase family member 10 OS=Mus musculus (Mouse) OX=10090 GN=Acad10 PE=1 SV=1	Q8K370	Acad10	119 kDa	0	16.747	
40	IF rod domain-containing protein OS=Mus musculus (Mouse) OX=10090 GN=Krt78 PE=1 SV=1	E9Q0F0	Krt78	112 kDa	9.2339	15.551	1.68
41	Protein TSSC4 OS=Mus musculus (Mouse) OX=10090 GN=Tssc4 PE=1 SV=1	Q9JHE7	Tssc4	34 kDa	9.2339	15.551	1.68
42	Hemoglobin subunit alpha OS=Mus musculus (Mouse) OX=10090 GN=Hba PE=1 SV=2	P01942	Hba	15 kDa	12.004	15.551	1.30
43	(E3-independent) E2 ubiquitin-conjugating enzyme UBE2O OS=Mus musculus (Mouse) OX=10090 GN=Ube2o PE=1 SV=3	Q6ZPJ3	Ube2o	141 kDa	8.3105	14.355	1.73
44	Peroxiredoxin-1 OS=Mus musculus (Mouse) OX=10090 GN=Prdx1 PE=1 SV=1	P35700	Prdx1	22 kDa	9.2339	14.355	1.55
45	60S acidic ribosomal protein P2 OS=Mus musculus (Mouse) OX=10090 GN=Rplp2 PE=1 SV=3	P99027	Rplp2	12 kDa	10.157	14.355	1.41
46	Transcriptional activator protein Pur-beta OS=Mus musculus (Mouse) OX=10090 GN=Purb PE=1 SV=3	O35295	Purb	34 kDa	9.2339	13.158	1.42
47	Calmodulin-1 OS=Mus musculus (Mouse) OX=10090 GN=Calm1 PE=1 SV=1	P0DP26	Calm1	17 kDa	5.5403	11.962	2.16
48	Cytochrome b-c1 complex subunit 6, mitochondrial OS=Mus musculus (Mouse) OX=10090 GN=Uqcrh PE=1 SV=2	P99028	Uqcrh	10 kDa	5.5403	11.962	2.16
49	Histone H2B type 1-F/J/L OS=Mus musculus (Mouse) OX=10090 GN=H2bc7 PE=1 SV=2	P10853	H2bc7	14 kDa	6.4637	11.962	1.85
50	cAMP-dependent protein kinase type II-alpha regulatory subunit OS=Mus musculus (Mouse) OX=10090 GN=Prkar2a PE=1 SV=2	P12367	Prkar2a	45 kDa	5.5403	10.766	1.94
51	AP-3 complex subunit sigma-2 OS=Mus musculus (Mouse) OX=10090 GN=Ap3s2 PE=1 SV=1	Q8BSZ2	Ap3s2	22 kDa	7.3871	10.766	1.46
52	Elongation factor 1-alpha 2 OS=Mus musculus (Mouse) OX=10090 GN=Eef1a2 PE=1 SV=1	P62631	Eef1a2	50 kDa	7.3871	10.766	1.46
53	Small nuclear ribonucleoprotein Sm D2 OS=Mus musculus (Mouse) OX=10090 GN=Snrpd2 PE=1 SV=1	P62317	Snrpd2	14 kDa	8.3105	10.766	1.30
54	Enhancer of rudimentary homolog OS=Mus musculus (Mouse) OX=10090 GN=Erh PE=1 SV=1	P84089	Erh	12 kDa	5.5403	9.5698	1.73
55	14-3-3 protein gamma OS=Mus musculus (Mouse) OX=10090 GN=Ywhag PE=1 SV=2	P61982	Ywhag	28 kDa	6.4637	9.5698	1.48
56	Beta-enolase OS=Mus musculus (Mouse) OX=10090 GN=Eno3 PE=1 SV=3	P21550	Eno3	47 kDa	6.4637	9.5698	1.48
57	Junctophilin-2 OS=Mus musculus (Mouse) OX=10090 GN=Jph2 PE=1 SV=2	Q9ET78	Jph2	75 kDa	6.4637	9.5698	1.48
58	Ribosome-binding protein 1 OS=Mus musculus (Mouse) OX=10090 GN=Rrbp1 PE=1 SV=2	Q99PL5	Rrbp1	173 kDa	6.4637	9.5698	1.48
59	Serine/threonine-protein phosphatase 2A catalytic subunit alpha isoform OS=Mus musculus (Mouse) OX=10090 GN=Ppp2ca PE=1 SV=1	P63330	Ppp2ca	36 kDa	6.4637	9.5698	1.48
60	Huntingtin-interacting protein K OS=Mus musculus (Mouse) OX=10090 GN=Hypk PE=1 SV=2	Q9CR41	Hypk	15 kDa	7.3871	9.5698	1.30
61	Complement C1q and tumor necrosis factor-related protein 9 OS=Mus musculus (Mouse) OX=10090 GN=C1qtnf9 PE=1 SV=1	Q4ZJN1	C1qtnf9	35 kDa	3.6936	8.3736	2.27
62	NADH dehydrogenase [ubiquinone] 1 beta subcomplex subunit 11, mitochondrial OS=Mus musculus (Mouse) OX=10090 GN=Ndufb11 PE=1 SV=2	O09111	Ndufb11	17 kDa	5.5403	8.3736	1.51
63	2-oxoisovalerate dehydrogenase subunit beta, mitochondrial OS=Mus musculus (Mouse) OX=10090 GN=Bckdhb PE=1 SV=2	Q6P3A8	Bckdhb	43 kDa	6.4637	8.3736	1.30

Supplemetary Table 1 (continued): Protein identified by mass spectomatry analysis

#	Identified Proteins (750)	Accession Number	ID	Molecular Weight	circNeg	circSLC8A1	Fold change
64	ATP synthase subunit epsilon, mitochondrial OS=Mus musculus (Mouse) OX=10090 GN=Atp5f1e PE=1 SV=2	P56382	Atp5f1e	6 kDa	6.4637	8.3736	1.30
65	Thioredoxin-dependent peroxide reductase, mitochondrial OS=Mus musculus (Mouse) OX=10090 GN=Prdx3 PE=1 SV=1	P20108	Prdx3	28 kDa	6.4637	8.3736	1.30
66	Poly(U)-binding-splicing factor PUF60 OS=Mus musculus (Mouse) OX=10090 GN=Puf60 PE=1 SV=2	Q3UEB3	Puf60	60 kDa	2.7702	7.1774	2.59
67	AP-2 complex subunit sigma OS=Mus musculus (Mouse) OX=10090 GN=Ap2s1 PE=1 SV=1	P62743	Ap2s1	17 kDa	3.6936	7.1774	1.94
68	Protein NDRG2 OS=Mus musculus (Mouse) OX=10090 GN=Ndrg2 PE=1 SV=1	Q9QYG0	Ndrg2	41 kDa	3.6936	7.1774	1.94
69	Serine/arginine-rich splicing factor 7 OS=Mus musculus (Mouse) OX=10090 GN=Srsf7 PE=1 SV=1	Q8BL97	Srsf7	31 kDa	3.6936	7.1774	1.94
70	Pre-mRNA-processing factor 40 homolog A OS=Mus musculus (Mouse) OX=10090 GN=Prpf40a PE=1 SV=1	Q9R1C7	Prpf40a	108 kDa	4.617	7.1774	1.55
71	Sorbin and SH3 domain-containing protein 2 OS=Mus musculus (Mouse) OX=10090 GN=Sorbs2 PE=1 SV=2	Q3UTJ2	Sorbs2	132 kDa	4.617	7.1774	1.55
72	Transket_pyr domain-containing protein OS=Mus musculus (Mouse) OX=10090 GN=Ogdhl PE=1 SV=1	E9Q7L0	Ogdhl	117 kDa	4.617	7.1774	1.55
73	Glutaredoxin-related protein 5, mitochondrial OS=Mus musculus (Mouse) OX=10090 GN=Glrx5 PE=1 SV=2	Q80Y14	Glrx5	16 kDa	5.5403	7.1774	1.30
74	Cysteine-rich protein 2 OS=Mus musculus (Mouse) OX=10090 GN=Crip2 PE=1 SV=1	Q9DCT8	Crip2	23 kDa	0	5.9811	
75	Elongation factor 1-beta OS=Mus musculus (Mouse) OX=10090 GN=Eef1b PE=1 SV=5	O70251	Eef1b	25 kDa	1.8468	5.9811	3.24
76	ATP synthase subunit f, mitochondrial OS=Mus musculus (Mouse) OX=10090 GN=Atp5mf PE=1 SV=3	P56135	Atp5mf	10 kDa	2.7702	5.9811	2.16
77	NADH dehydrogenase [ubiquinone] 1 alpha subcomplex assembly factor 3 OS=Mus musculus (Mouse) OX=10090 GN=Ndufaf3 PE=1 SV=1	Q9JKL4	Ndufaf3	21 kDa	2.7702	5.9811	2.16
78	Transformer-2 protein homolog beta OS=Mus musculus (Mouse) OX=10090 GN=Tra2b PE=1 SV=1	P62996	Tra2b	34 kDa	2.7702	5.9811	2.16
79	Lipoprotein lipase OS=Mus musculus (Mouse) OX=10090 GN=Lpl PE=1 SV=3	P11152	Lpl	53 kDa	3.6936	5.9811	1.62
80	NADH dehydrogenase [ubiquinone] 1 alpha subcomplex subunit 2 OS=Mus musculus (Mouse) OX=10090 GN=Ndufa2 PE=1 SV=3	Q9CQ75	Ndufa2	11 kDa	4.617	5.9811	1.30
81	Cytochrome c1, heme protein, mitochondrial OS=Mus musculus (Mouse) OX=10090 GN=Cyc1 PE=1 SV=1	Q9D0M3	Cyc1	35 kDa	0	4.7849	
82	NADH dehydrogenase [ubiquinone] 1 beta subcomplex subunit 9 OS=Mus musculus (Mouse) OX=10090 GN=Ndufb9 PE=1 SV=3	Q9CQJ8	Ndufb9	22 kDa	0	4.7849	
83	Mitochondrial import receptor subunit TOM22 homolog OS=Mus musculus (Mouse) OX=10090 GN=Tomm22 PE=1 SV=3	Q9CPQ3	Tomm22	16 kDa	1.8468	4.7849	2.59
84	NADH dehydrogenase [ubiquinone] 1 alpha subcomplex subunit 7 OS=Mus musculus (Mouse) OX=10090 GN=Ndufa7 PE=1 SV=3	Q9Z1P6	Ndufa7	13 kDa	1.8468	4.7849	2.59
85	26S proteasome non-ATPase regulatory subunit 9 OS=Mus musculus (Mouse) OX=10090 GN=Psmd9 PE=1 SV=1	Q9CR00	Psmd9	25 kDa	2.7702	4.7849	1.73
86	H/ACA ribonucleoprotein complex subunit 2 OS=Mus musculus (Mouse) OX=10090 GN=Nhp2 PE=1 SV=1	Q9CRB2	Nhp2	17 kDa	2.7702	4.7849	1.73
87	Histone H2A type 2-A OS=Mus musculus (Mouse) OX=10090 GN=Hist2h2aa1 PE=1 SV=3	Q6GSS7	Hist2h2aa1	14 kDa	2.7702	4.7849	1.73
88	Serine/arginine-rich splicing factor 1 OS=Mus musculus (Mouse) OX=10090 GN=Srsf1 PE=1 SV=3	Q6PDM2	Srsf1	28 kDa	2.7702	4.7849	1.73
89	60S acidic ribosomal protein P1 OS=Mus musculus (Mouse) OX=10090 GN=Rplp1 PE=1 SV=1	P47955	Rplp1	11 kDa	3.6936	4.7849	1.30
90	Cytochrome c oxidase subunit 7A1, mitochondrial OS=Mus musculus (Mouse) OX=10090 GN=Cox7a1 PE=1 SV=1	P56392	Cox7a1	9 kDa	3.6936	4.7849	1.30
91	DNA-directed RNA polymerases I, II, and III subunit RPABC3 OS=Mus musculus (Mouse) OX=10090 GN=Polr2h PE=1 SV=3	Q923G2	Polr2h	17 kDa	3.6936	4.7849	1.30
92	Long-chain specific acyl-CoA dehydrogenase, mitochondrial OS=Mus musculus (Mouse) OX=10090 GN=Acadl PE=1 SV=2	P51174	Acadl	48 kDa	3.6936	4.7849	1.30
93	Metaxin-2 OS=Mus musculus (Mouse) OX=10090 GN=Mtx2 PE=1 SV=1	O88441	Mtx2	30 kDa	3.6936	4.7849	1.30
94	Scaffold attachment factor B1 OS=Mus musculus (Mouse) OX=10090 GN=Safb PE=1 SV=2	D3YXK2	Safb	105 kDa	3.6936	4.7849	1.30
95	Serine/threonine-protein phosphatase 2A 55 kDa regulatory subunit B alpha isoform OS=Mus musculus (Mouse) OX=10090 GN=Ppp2r2a PE=1 SV=1	Q6P1F6	Ppp2r2a	52 kDa	3.6936	4.7849	1.30
96	Desmoplakin OS=Mus musculus (Mouse) OX=10090 GN=Dsp PE=1 SV=1	E9Q557	Dsp	333 kDa	0	3.5887	
97	Guanine nucleotide-binding protein G(I)/G(S)/G(T) subunit beta-1 OS=Mus musculus (Mouse) OX=10090 GN=Gnb1 PE=1 SV=3	P62874	Gnb1	37 kDa	0	3.5887	
98	Kinesin heavy chain isoform 5C OS=Mus musculus (Mouse) OX=10090 GN=Kif5c PE=1 SV=3	P28738	Kif5c	109 kDa	0	3.5887	
99	Chromobox protein homolog 3 OS=Mus musculus (Mouse) OX=10090 GN=Cbx3 PE=1 SV=2	P23198	Cbx3	21 kDa	1.8468	3.5887	1.94
100	Eukaryotic translation initiation factor 3 subunit F OS=Mus musculus (Mouse) OX=10090 GN=Eif3f PE=1 SV=2	Q9DCH4	Eif3f	38 kDa	1.8468	3.5887	1.94
101	KH domain-containing, RNA-binding, signal transduction-associated protein 1 OS=Mus musculus (Mouse) OX=10090 GN=Khdrbs1 PE=1 SV=2	Q60749	Khdrbs1	48 kDa	1.8468	3.5887	1.94
102	Latexin OS=Mus musculus (Mouse) OX=10090 GN=Lxn PE=1 SV=2	P70202	Lxn	25 kDa	1.8468	3.5887	1.94
103	Thrombospondin type-1 domain-containing protein 7A OS=Mus musculus (Mouse) OX=10090 GN=Thsd7a PE=1 SV=2	Q69ZU6	Thsd7a	184 kDa	1.8468	3.5887	1.94
104	U1 small nuclear ribonucleoprotein A OS=Mus musculus (Mouse) OX=10090 GN=Snrpa PE=1 SV=3	Q62189	Snrpa	32 kDa	1.8468	3.5887	1.94
105	Vitamin D-binding protein OS=Mus musculus (Mouse) OX=10090 GN=Gc PE=1 SV=2	P21614	Gc	54 kDa	1.8468	3.5887	1.94
106	40S ribosomal protein S21 OS=Mus musculus (Mouse) OX=10090 GN=Rps21 PE=1 SV=1	Q9CQR2	Rps21	9 kDa	0	2.3925	
107	Acetyl-CoA carboxylase 2 OS=Mus musculus (Mouse) OX=10090 GN=Acacb PE=1 SV=1	E9Q4Z2	Acacb	276 kDa	0	2.3925	
108	Actin-binding LIM protein 1 OS=Mus musculus (Mouse) OX=10090 GN=Ablim1 PE=1 SV=1	Q8K4G5	Ablim1	97 kDa	0	2.3925	
109	Actin-related protein 2/3 complex subunit 2 OS=Mus musculus (Mouse) OX=10090 GN=Arpc2 PE=1 SV=3	Q9CVB6	Arpc2	34 kDa	0	2.3925	
110	Bridging integrator 2 OS=Mus musculus (Mouse) OX=10090 GN=Bin2 PE=1 SV=1	D3Z6Q9	Bin2	53 kDa	0	2.3925	
111	Cadherin-13 OS=Mus musculus (Mouse) OX=10090 GN=Cdh13 PE=1 SV=2	Q9WTR5	Cdh13	78 kDa	0	2.3925	
112	COP9 signalosome complex subunit 8 OS=Mus musculus (Mouse) OX=10090 GN=Cops8 PE=1 SV=1	Q8VBV7	Cops8	23 kDa	0	2.3925	
113	E3 ubiquitin-protein ligase RMND5A OS=Mus musculus (Mouse) OX=10090 GN=Rmnd5a PE=1 SV=2	Q80YQ8	Rmnd5a	44 kDa	0	2.3925	
114	Glutaryl-CoA dehydrogenase, mitochondrial OS=Mus musculus (Mouse) OX=10090 GN=Gcdh PE=1 SV=2	Q60759	Gcdh	49 kDa	0	2.3925	
115	Histidine-rich calcium-binding protein OS=Mus musculus (Mouse) OX=10090 GN=Hrc PE=1 SV=1	G5E8J6	Hrc	85 kDa	0	2.3925	
116	NADH dehydrogenase [ubiquinone] 1 alpha subcomplex subunit 9, mitochondrial OS=Mus musculus (Mouse) OX=10090 GN=Ndufa9 PE=1 SV=2	Q9DC69	Ndufa9	43 kDa	0	2.3925	
117	Predicted gene 11639 OS=Mus musculus (Mouse) OX=10090 GN=Gm11639 PE=1 SV=1	A0A1D5RLM8-DECOY			0	2.3925	
118	Protein phosphatase 1A OS=Mus musculus (Mouse) OX=10090 GN=Ppm1a PE=1 SV=1	P49443	Ppm1a	42 kDa	0	2.3925	
119	Ribose-phosphate diphosphokinase OS=Mus musculus (Mouse) OX=10090 GN=Prps1l1 PE=1 SV=1	Q8C5R8	Prps1l1	35 kDa	0	2.3925	
120	Synaptopodin-2 OS=Mus musculus (Mouse) OX=10090 GN=Synpo2 PE=1 SV=2	Q91YE8	Synpo2	117 kDa	0	2.3925	
121	Translocon-associated protein subunit alpha OS=Mus musculus (Mouse) OX=10090 GN=Ssr1 PE=1 SV=1	Q9CY50	Ssr1	32 kDa	0	2.3925	

Note: Red labeled proteins are mitochondrial proteins.

Supplementary Table S2: Primer information.

Name		Sequence
circSlc8a1/cA-circSlc8a1-1	Forward:	5’-ctattgaaggcacagcccgagg-3'
	Reverse:	5’-gtacaataagacttccaactgc-3'
circSlc8a1/cA-circSlc8a1-2	Forward:	5'-acagcccgaggtggaggggaagac-3'
	Reverse:	5'-ggtgggagacttaatcgaagcatg-3'
Slc8a1 mRNA	Forward:	5’ gagcagccttcagagctggtcgg-3’
	Reverse:	5’-gtacaataagacttccaactgc-3'
RNU6	Forward:	5'-gtgctcgcttcggcagcacata-3'
	Reverse:	5'-tggaacgcttcacgaatttgcg-3'
Gapdh	Forward:	5’-cccacttgaagggtggagcc-3'
	Reverse:	5’-acaatcttgagtgagttgtc-3'
cA-circSlc8a1 precursor	Forward:	5'-acagcccgaggtggaggggaagac-3'
	Reverse:	5'-gagctgtcagagatttctccaacc-3'
cA-circSlc8a1 genotyping	Forward:	5’gggcccgcctcgagacacttagccgtgttctt-3'
	Reverse:	5'-ggtgggagacttaatcgaagcatg-3'
circSlc8a1 genotyping	Forward:	5'-tgtggagagctcgaattccagaa-3
	Reverse:	5'-gcatgcatagatcttacggaaaacggcagaag-3'
collagen1a1	Forward:	5’-gaatggagatgatggggaagctgg-3'
	Reverse:	5’-catctcctttggcaccatccaaac-3'
collagen3a1	Forward:	5’-gtaaagaagtctctgaagctgatg-3'
	Reverse:	5’-gcgatatctatgatgggtagtctc-3'
ANP	Forward:	5’-gcggtgtccaacacagatctgatg-3'
	Reverse:	5’-ggtgggttgacctccccagtccag-3'
BNP	Forward:	5’-gagcaattcaagatgcaggtgagc-3'
	Reverse:	5’-cacacacacctgaatcccccatcc-3'

Supplementary Table S3

Construct sequences

cA-circSlc8a1

ccagttgttcaactcacccttcagattaaaaataactgaggtaagggcctgggtaggggaggtggtgtgagacgctcctgtctctcctctatctgcccatcggccctttggggaggaggaatgtgcccaaggactaaaaaaaggccatggagcca
gaggggcgagggcaacagacctttcatgggcaaaccttggggccctgctgtcctcctgtcacctccagagccaagggatcaaaggaggaggagccaggacaggagggaagtgggagggagggtcccagcagaggactccaaatttaggc
agcaggcatatgggatgggatataaaggggctggagcactgagagctgtcagagatttctccaacccgtcgacacacttagccgtgttctttgcacttctgcatgtcccccgtctggcctggctgtccccagtggcttccccagtgt
gacatggtgcatctctgccttacaggaattcgagctctccacaggtgtcctcaaagtcttcccctccacctcgggctgtgccttcaatagttttgtagggaatgataacatttcctcgagctccagaggttctcaaaaccttcacctccatgatgcca
atgctctcgctcacgtgagtcacgggttcctcaaatgtaaagatgcctgcatggtcatcatcaaaaatggttatggtggcagtgctgggtgacccaagacaagcaattgaagaagcgtgattggattctagtatgccatcttctgaaacatctgaaga
gactctgacattgctaagatgcacaaggaagttttcatcttcttcaaagatatcatcatcaatgatgccaactctgatttccttctgggtctcccctggtttgaagatcacagtcccttccgtgaattcataatcagacccagcattggctgtgccgtcttctg
tcctgaagtcaacaaacacagtggtgctcaagtcgcccccctctgcgcataatggtgagggccacagtaccacagttctctagacactggtatgttccttgctcaaagaagatcttactgactgggtcgttttcagccatttccatgttgacttcatgcata
ctgacagccttccttgcttgatcagctgcgtgcctcttcaagatgttgccagctccggtcatcaggcgagtagcttgaatcctgtaaaatgctcggcttttctgctgttgacttaggacctggtagttggctaattctattaattgctcaatttctttctcagga
tgcttctgcttaagttccttcagaatccttgccatctcacgcctggcttcctcatcatcttggtccctctcatcaacttccaaaaccagagccccatctaagaaattgtcaacatgagagttgaccactttcccatccatttcgatttcagttttggaagctggt
ctgtctccttcatgttcaatgatcatcccccctctgcttgccggccctgtaccgcttgtagacatacttgtaaaagagaagccgcctgtctgctacccacgcgaacacaacgcagatgggaaagaagaagaaagtaagcaagccttcccagacctcca
caactccaggagagctgacagacaagattatataaagccaggtataggcaaagatgctccaggctgctgtcacaaagaacacacgcagatgcttgatcttccttgtctctccatcagggaccacgtaaacacagagtgcgattatgatgaacatgtt
aaaggcagcacttcccacgatggtgctgggacccaggtcccctgcggtgaagttatggccgcacacttcaatgactgacaggagaatctcaggagcagaagatcccagggccatcaaggtcaggttcgacacagtctcgttccagattctcacc
gtcgtcttggtggtctctccattcggtttctttatcgttatttctttctcttgagaggtgatgacctctatagaggacataaaccggtctgcaataatagaaactccaaggaacatgtagaccatggccacaaaatacacagttgctctagcaattttgtcccc
aaaagatgggtcttggggttcccaaatgggcaagatcacccctttcttacagtaatatgagccagtacattcagtggtttcatttcctcctgtttctgcctctgtatctgcagttatatggtcaacatgggaaaacaagagagccaccagagctaccaga
cgaaatcccattgaaacattgggtgggagacttaatcgaagcatgttgtacaataagacttccaactgctccaacactatttcatcgttctggtgagtggcccgctacctcttctggtggccgcctccctccttcctggcctcccggagctg
cgcccttctcactggttctctcttctgccgttttccgtaggatcct

circSlc8a1

tgtcgacacacttagccgtgttctttgcacttctgcatgtcccccgtctggcctggctgtccccagtggcttccccagtgtgacatggtgcatctctgccttacaggttggagcagttggaagtcttattgtacaacatgcttcgatt
aagtctcccacccaatgtttcaatgggatttcgtctggtagctctggtggctctcttgttttcccatgttgaccatataactgcagatacagaggcagaaacaggaggaaatgaaaccactgaatgtactggctcatattactgtaagaaaggggtgatc
ttgcccatttgggaaccccaagacccatcttttggggacaaaattgctagagcaactgtgtatttttgtggccatggtctacatgttccttggagtttctattattgcagaccggtttatgtcctctatagaggtcatcacctctcaagagaaagaaataacg
ataaagaaaccgaatggagagaccaccaagacgacggtgagaatctggaacgagactgtgtcgaacctgaccttgatggccctgggatcttctgctcctgagattctcctgtcagtcattgaagtgtgcggccataacttcaccgcaggggacct
gggtcccagcaccatcgtgggaagtgctgcctttaacatgttcatcataatcgcactctgtgtttacgtggtccctgatggagagacaaggaagatcaagcatctgcgtgtgttctttgtgacagcagcctggagcatctttgcctatacctggctttat
ataatcttgtctgtcagctctcctggagttgtggaggtctgggaaggcttgcttacttttcttcttctttcccatctgcgttgtgttcgcgtgggtagcagacaggcggcttctcttttacaagtatgtctacaagcggtacagggccggcaagcagaggggg
gatgatcattgaacatgaaggagacagaccagcttccaaaactgaaatcgaaatggatgggaaagtggtcaactctcatgttgacaatttcttagatggggctctggttttggaagttgatgagagggaccaagatgatgaggaagccaggcgtga
gatggcaaggattctgaaggaacttaagcagaagcatcctgagaaagaaattgagcaattaatagaattagccaactaccaggtcctaagtcaacagcagaaaagccgagcattttacaggattcaagctactcgcctgatgaccggagctggca
acatcttgaagaggcacgcagctgatcaagcaaggaaggctgtcagtatgcatgaagtcaacatggaaatggctgaaaacgacccagtcagtaagatcttctttgagcaaggaacataccagtgtctagagaactgtggtactgtggccctcacc
attatgcgcagagggggcgacttgagcaccactgtgtttgttgacttcaggacagaagacggcacagccaatgctgggtctgattatgaattcacggaagggactgtgatcttcaaaccaggggagacccagaaggaaatcagagttggcatcat
tgatgatgatatctttgaagaagatgaaaacttccttgtgcatcttagcaatgtcagagtctcttcagatgtttcagaagatggcatactagaatccaatcacgcttcttcaattgcttgtcttgggtcacccagcactgccaccataaccatttttgatgatg
accatgcaggcatcttacatttgaggaacccgtgactcacgtgagcgagagcattggcatcatggaggtgaaggttttgagaacctctggagctcgaggaaatgttatcattccctacaaaactattgaaggcacagcccgaggtggaggggaa
gactttgaggacacctgtggagagctcgaattccagaacgatgaaatagtgtgagtggcccgctacctcttctggtggccgcctccctccttcctggcctcccggagctgcgcccctttctcactggttctctcttctgccgttttccgt
aggatcct

pre-cA-circSlc. cA-circSlc8a1-intron mutation (producing pre-c*A-circSlc8a1*).

Ccagttgttcaactcacccttcagattaaaaataactgaggtaagggcctgggtaggggaggtggtgtgagacgctcctgtctctcctctatctgcccatcggccctttggggaggaggaatgtgcccaaggactaaaaaaaggccatggagcca
gaggggcgagggcaacagacctttcatgggcaaaccttggggccctgctgtcctcctgtcacctccagagccaagggatcaaaggaggaggagccaggacaggagggaagtgggagggagggtcccagcagaggactccaaatttaggc
agcaggcatatgggatgggatataaaggggctggagcactgagagctgtcagagatttctccaaccc
Gtcgac acacttagccgtgttctttgcacttctgcatgtcccccgtctggcctggctgtccccagtggcttccccagtgtgacataaatttaattaaaaaatttt
gaattcgagctctccacaggtgtcctcaaagtcttcccctccacctcgggctgtgccttcaatagttttgtagggaatgataacatttcctcgagctccagaggttctcaaaaccttcacctccatgatgccaatgctctcgctcacgtgagtcacgggtt
cctcaaatgtaaagatgcctgcatggtcatcatcaaaaatggttatggtggcagtgctgggtgacccaagacaagcaattgaagaagcgtgattggattctagtatgccatcttctgaaacatctgaagagactctgacattgctaagatgcacaagg
aagttttcatcttcttcaaagatatcatcatcaatgatgccaactctgatttccttctgggtctcccctggtttgaagatcacagtcccttccgtgaattcataatcagacccagcattggctgtgccgtcttctgtcctgaagtcaacaaacacagtggtgct
caagtcgcccccctctgcgcataatggtgagggccacagtaccacagttctctagacactggtatgttccttgctcaaagaagatcttactgactgggtcgttttcagccatttccatgttgacttcatgcatactgacagccttccttgcttgatcagctgc
gtgcctcttcaagatgttgccagctccggtcatcaggcgagtagcttgaatcctgtaaaatgctcggcttttctgctgttgacttaggacctggtagttggctaattctattaattgctcaatttctttctcaggatgcttctgcttaagttccttcagaatccttg
ccatctcacgcctggcttcctcatcatcttggtccctctcatcaacttccaaaaccagagccccatctaagaaattgtcaacatgagagttgaccactttcccatccatttcgatttcagttttggaagctggtctgtctccttcatgttcaatgatcatccccc
tctgcttgccggccctgtaccgcttgtagacatacttgtaaaagagaagccgcctgtctgctacccacgcgaacacaacgcagatgggaaagaagaagaaagtaagcaagccttcccagacctccacaactccaggagagctgacagacaagaat
tatataaagccaggtataggcaaagatgctccaggctgctgtcacaaagaacacacgcagatgcttgatcttccttgtctctccatcagggaccacgtaaacacagagtgcgattatgatgaacatgttaaaggcagcacttcccacgatggtgctgg
gacccaggtcccctgcggtgaagttatggccgcacacttcaatgactgacaggagaatctcaggagcagaagatcccagggccatcaaggtcaggttcgacacagtctcgttccagattctcaccgtcgtcttggtggtctctccattcggtttcttta
tcgttatttctttctcttgagaggtgatgacctctatagaggacataaaccggtctgcaataatagaaactccaaggaacatgtagaccatggccacaaaatacacagttgctctagcaattttgtcccccaaaagatgggtcttggggttcccaaatggg
caagatcacccctttcttacagtaatatgagccagtacattcagtggtttcatttcctcctgtttctgcctctgtatctgcagttatatggtcaacatgggaaaacaagagagccaccagagctaccagacgaaatcccattgaaacattgggtgggagac
ttaatcgaagcatgttgtacaataagacttccaactgctccaacactatttcatcgttctggtgagtggcccgctacctcttctggtggccgcctccctccttcctggcctcccggagctgcgcccctttctcactggttctctcttctgccgt
tttccgtaggatcct

pre-circSlc. *circSlc8a1-*intron mutation (producing pre-c*ircSlc8a1*).

tgtcgacacacttagccgtgttctttgcacttctgcatgtcccccgtctggcctggctgtccccagtggcttccccagtgtgacataaatttaattaaaaaatttttgttggagcagttggaagtcttattgtacaacatgcttcgattaagtctcccaccca
atgtttcaatgggatttcgtctggtagctctggtggctctcttgttttcccatgttgaccatataactgcagatacagaggcagaaacaggaggaaatgaaaccactgaatgtactggctcatattactgtaagaaaggggtgatcttgcccatttggga
accccaagacccatcttttggggacaaaattgctagagcaactgtgtatttttgtggccatggtctacatgttccttggagtttctattattgcagaccggtttatgtcctctatagaggtcatcacctctcaagagaaagaaataacgataaagaaaccga
atggagagaccaccaagacgacggtgagaatctggaacgagactgtgtcgaacctgaccttgatggccctgggatcttctgctcctgagattctcctgtcagtcattgaagtgtgcggccataacttcaccgcaggggacctgggtcccagcacc
atcgtgggaagtgctgcctttaacatgttcatcataatcgcactctgtgtttacgtggtccctgatggagagacaaggaagatcaagcatctgcgtgtgttctttgtgacagcagcctggagcatctttgcctatacctggctttatataatcttgtctgtca
gctctcctggagttgtggaggtctgggaaggcttgcttacttttcttcttctttcccatctgcgttgtgttcgcgtgggtagcagacaggcggcttctcttttacaagtatgtctacaagcggtacagggccggcaagcagaggggatgatcattgaac
atgaaggagacagaccagcttccaaaactgaaatcgaaatggatgggaaagtggtcaactctcatgttgacaatttcttagatggggctctggttttggaagttgatgagagggaccaagatgatgaggaagccaggcgtgagatggcaaggatt
ctgaaggaacttaagcagaagcatcctgagaaagaaattgagcaattaatagaattagccaactaccaggtcctaagtcaacagcagaaaagccgagcattttacaggattcaagctactcgcctgatgaccggagctggcaacatcttgaagag
gcacgcagctgatcaagcaaggaaggctgtcagtatgcatgaagtcaacatggaaatggctgaaaacgacccagtcagtaagatcttctttgagcaaggaacataccagtgtctagagaactgtggtactgtggccctcaccattatgcgcagag
ggggcgacttgagcaccactgtgtttgttgacttcaggacagaagacggcacagccaatgctgggtctgattatgaattcacggaagggactgtgatcttcaaaccaggggagacccagaaggaaatcagagttggcatcattgatgatgatatct
ttgaagaagatgaaaacttccttgtgcatcttagcaatgtcagagtctcttcagatgtttcagaagatggcatactagaatccaatcacgcttcttcaattgcttgtcttgggtcacccagcactgccaccataaccatttttgatgatgaccatgcaggcat
ctttacatttgaggaacccgtgactcacgtgagcgagagcattggcatcatggaggtgaaggttttgagaacctctggagctcgaggaaatgttatcattccctacaaaactattgaaggcacagcccgaggtggaggggaagacttt gaggaca
cctgtggagagctcgaattccagaacgatgaaatagtgtgagtggcccgctacctcttctggtggccgcctccctccttcctggcctcccggagctgcgcccctttctcactggttctctcttctgccgttttccgtaggatcct

Probe sequences

circSlc8a1 probe: 5’ agacttccaactgctccaacactatttcatcgttgaa-3’

cA-circSlc8a1 probe: 5’ cctgtggagagctcgaattccagaacgatgaaatagtgtt-3’